U.S. ARMY

ARL

RESEARCH LABORATORY

Computerized Design, Generation, Simulation of Meshing and Contact, and Stress Analysis of Formate Cut Spiral Bevel Gear Drives

Faydor L. Litvin and Alfonso Fuentes
University of Illinois at Chicago, Chicago, Illinois

Baxter R. Mullins and Ron Woods
Bell Helicopter Textron, Inc., Forth Worth, Texas

20030910 096

Since its founding, NASA has been dedicated to the advancement of aeronautics and space science. The NASA Scientific and Technical Information (STI) Program Office plays a key part in helping NASA maintain this important role.

The NASA STI Program Office is operated by Langley Research Center, the Lead Center for NASA's scientific and technical information. The NASA STI Program Office provides access to the NASA STI Database, the largest collection of aeronautical and space science STI in the world. The Program Office is also NASA's institutional mechanism for disseminating the results of its research and development activities. These results are published by NASA in the NASA STI Report Series, which includes the following report types:

- TECHNICAL PUBLICATION. Reports of completed research or a major significant phase of research that present the results of NASA programs and include extensive data or theoretical analysis. Includes compilations of significant scientific and technical data and information deemed to be of continuing reference value. NASA's counterpart of peer-reviewed formal professional papers but has less stringent limitations on manuscript length and extent of graphic presentations.

- TECHNICAL MEMORANDUM. Scientific and technical findings that are preliminary or of specialized interest, e.g., quick release reports, working papers, and bibliographies that contain minimal annotation. Does not contain extensive analysis.

- CONTRACTOR REPORT. Scientific and technical findings by NASA-sponsored contractors and grantees.

- CONFERENCE PUBLICATION. Collected papers from scientific and technical conferences, symposia, seminars, or other meetings sponsored or cosponsored by NASA.

- SPECIAL PUBLICATION. Scientific, technical, or historical information from NASA programs, projects, and missions, often concerned with subjects having substantial public interest.

- TECHNICAL TRANSLATION. English-language translations of foreign scientific and technical material pertinent to NASA's mission.

Specialized services that complement the STI Program Office's diverse offerings include creating custom thesauri, building customized databases, organizing and publishing research results . . . even providing videos.

For more information about the NASA STI Program Office, see the following:

- Access the NASA STI Program Home Page at *http://www.sti.nasa.gov*

- E-mail your question via the Internet to help@sti.nasa.gov

- Fax your question to the NASA Access Help Desk at 301–621–0134

- Telephone the NASA Access Help Desk at 301–621–0390

- Write to:
  NASA Access Help Desk
  NASA Center for AeroSpace Information
  7121 Standard Drive
  Hanover, MD 21076

Computerized Design, Generation, Simulation of Meshing and Contact, and Stress Analysis of Formate Cut Spiral Bevel Gear Drives

Faydor L. Litvin and Alfonso Fuentes
University of Illinois at Chicago, Chicago, Illinois

Baxter R. Mullins and Ron Woods
Bell Helicopter Textron, Inc., Forth Worth, Texas

National Aeronautics and
Space Administration

Glenn Research Center

Available from

Computerized Design, Generation, Simulation of Meshing and Contact, and Stress Analysis of Formate Cut Spiral Bevel Gear Drives

Faydor L. Litvin* and Alfonso Fuentes
University of Illinois at Chicago
Gear Research Center, Department of Mechanical and Industrial Engineering
Chicago, Illinois 60607–7022

Baxter R. Mullins and Ron Woods
Bell Helicopter Textron, Inc.
Forth Worth, Texas 76101

Abstract

A new approach for design, generation, computerized simulation of meshing and contact, and stress analysis of formate cut spiral bevel gear drives is reported. The approach proposed is based on application of four procedures that permit in sequence to provide a longitudinally directed bearing contact, a predesigned parabolic function of transmission errors, a limit to the shift of bearing contact caused by errors of alignment, and to automatically generate the finite element models for application of a general purpose finite element analysis computer program. A new computer program has been developed that provides optimized machine-tool settings for finishing of spiral bevel gears utilizing the "Formate" grinding process with minimized transmission errors. The new computer program is based on the four procedures mentioned above. The developed theory is illustrated with several examples of design and computations.

Nomenclature

α_g	Profile angle of parabolic blade for gear head cutter at mean point M
α_p	Blade angle for straight blade of pinion head cutter
δ	Elastic approach of contacting surfaces
$\gamma_i (i = 1, 2)$	Pitch cone angles of pinion $(i = 1)$ and gear $(i = 2)$, respectively
$\gamma_{m_i} (i = 1, 2)$	Machine root angles for pinion $(i = 1)$ and gear $(i = 2)$, respectively
$\gamma_{r_i} (i = 1, 2)$	Root cone angles for pinion $(i = 1)$ and gear $(i = 2)$, respectively
γ	Shaft angle
$\eta_i (i = 1, 2)$	Tangent to the path of contact on the pinion $(i = 1)$ and gear $(i = 2)$ surface, respectively
θ_p, θ_g	Surface parameters of the pinion and gear head cutters, respectively
λ_f, λ_w	Surface parameters of the pinion and gear fillet parts of the head cutter
λ_f, λ_w	Surface parameters of the pinion and gear fillet parts of the head cutter
$\sigma^{(ij)}$	Angle formed between principal directions $(i, j = 1, 2, p, g)$
$\phi_i (i = 1, 2)$	Angle of rotation of the pinion $(i = 1)$ or gear $(i = 2)$ in the process of meshing
ψ_{c1}	Angle of rotation of the cradle in the process of generation of the pinion
ψ_1	Angle of rotation of the pinion in the process of generation
ρ_f, ρ_w	Fillet radii for the pinion and the gear
$\omega^{(1)}$	Angular velocity of the pinion (in meshing and generation)

Corresponding author: Phone: 312–996–2866, Fax: 312–413–0447, E-mail: FLitvin@uic.edu

Symbol	Definition
$\Sigma_i\,(i=1,2)$	Pinion $(i=1)$ or gear $(i=2)$ tooth surface
$\Sigma_k\,(k=p,g)$	Pinion $(k=p)$ or gear $(k=g)$ generating surface
$\Delta\phi_2(\phi_1)$	Function of transmission errors
$\Delta A_1, \Delta A_2$	Pinion and gear axial displacements, respectively
$\Delta E, \Delta\gamma$	Errors of the offset and shaft angle, respectively
a_c	Parabolic coefficient of gear head cutter blade
a_{d_1}	Dedendum of pinion
A_m, F_w	Mean cone distance and face width
b_i	Coefficients of modified roll for pinion generation $(i=1,2,3)$
$\mathbf{e}_f, \mathbf{e}_h, \mathbf{e}_s, \mathbf{e}_q$	Unit vectors of principal directions of pinion and gear tooth surfaces, respectively
$\mathbf{e}_t, \mathbf{e}_p, \mathbf{e}_g, \mathbf{e}_u$	Unit vectors of principal directions of the cutter surface for pinion and gear, respectively
E_{m_1}	Blank offset for pinion
$k_n^{(i)}$	Normal curvature of surface Σ_i
$k_n^{(r)}$	Relative normal curvature
k_f, k_h, k_s, k_q	Principal curvatures of pinion and gear tooth surfaces, respectively
k_t, k_p, k_g, k_u	Principal curvatures of cutter surfaces for pinion and gear, respectively
m'_{12}	Second derivative of transmission function $\phi_2(\phi_1)$
m_{12}	Gear ratio
M	Mean contact point
$\mathbf{M}_{ji}, \mathbf{L}_{ji}$	Matrices of coordinate transformation from system S_i to system S_j
$\mathbf{n}_i^{(k)}, \mathbf{N}_i^{(k)}$	Unit normal and normal to surface Σ_k represented in coordinate system S_i
$N_i\,(i=1,2)$	Tooth number of pinion $(i=1)$ or gear $(i=2)$
q_1	Installment angle for head cutter of the pinion
R_p, R_g	Radii of the head cutter at mean contact point for the pinion and gear
R_u	Gear cutter radius
$\mathbf{r}_i$	Position vector represented in system $S_i\;(i=1,2,b_1,b_2,h,l,m_1,m_2,p,g)$
s_p	Surface parameter of the pinion
S_i	Coordinate system $(i=1,2,b_1,b_2,h,l,m_1,m_2,p,g)$
S_{r_1}	Radial setting of the head-cutter of the pinion
u_g	Gear tooth surface parameter
$\mathbf{v}_r^{(k)}\,(k=p,g)$	Velocity of contact point in its motion over surface Σ_k
$\mathbf{v}_{tr}^{(i)}$	Transfer velocity of contact point in its motion with surface Σ_i
$\mathbf{v}^{(ij)}$	Relative velocity at contact point $(i,j=1,2,c_1,p)$
$v_s^{(i)}, v_a^{(i)}$	Components of the velocity of the contact point in its motion over Σ_i
X_{B_1}	Sliding base for pinion
X_{D_1}	Machine center to back for pinion
X_f, X_g	Center distances of fillet circular arcs of pinion and gear, respectively
X_G	Machine center to back for gear
$2a$	Length of major axis of contact ellipse

Chapter 1

Developed Theory

1.1 Introduction

Design and generation of spiral bevel gears is a subject of intensive research of scientists, designers, and manufacturers. High quality equipment such as CNC (computer numerically controlled) machines and tools have been produced by Gleason Works (USA) and Klingelnberg-Oerlikon (Germany and Switzerland) for precise manufacturing. However, the quality of spiral bevel gears depends substantially on the design of machine-tool settings that have to be determined for each design of spiral bevel gears. The machine-tool settings are not standardized and their determination is a subject of high quality research. The freedom of choosing optimized machine-tool settings allows us to generate low-noise stable bearing contact spiral bevel gears.

The subject of this research project is the enhanced design of formate cut spiral bevel gears. Formate is a Gleason Works trademark applied for nongenerated spiral bevel gears. The term "formate cut" means that the gear is held at rest and grinding or cutting wheel (head cutter) does not orbit the cradle. Thus, the gear tooth surface is a copy of the tool surface that is a surface of revolution (see Section 1.3). The pinion tooth surface is generated by a head-cutter while the tool and the pinion perform related rotations. The pinion tooth surface is generated as the envelope to the family of the tool (head-cutter) surfaces. The advantage of the formate-cut method is the high productivity of gear generation. The main problem of the design of formate-cut spiral bevel gears is the conjugation of tooth surfaces of the gear and the pinion.

The contents of the report cover: (i) computational procedures of the proposed approach that permit the design of a longitudinal bearing contact and a parabolic function of transmission errors, and investigation of the influence of errors of alignment; (ii) algorithms of computer programs developed for synthesis, analysis of meshing and contact, and automatic development of finite element models; (iii) results of computations for several cases of design of formate cut spiral bevel gear drives; and (iv) results of finite element analysis of several design cases of both face-milled generated and formate cut spiral bevel gear drives.

1.2 Basic Ideas of Proposed Approach

Localization of Contact. The contact of pinion-gear tooth surfaces is localized due to the mismatch of generating surfaces (surfaces of the head-cutters) that is achieved by application of different dimensions and profiles of the gear-pinion head-cutters.

The generated pinion-gear tooth surfaces are in point contact at every instant. The tooth contact under load is spread over an elliptical area and the bearing contact is formed as a set of contact ellipses. The magnitude and orientation of instantaneous contact ellipse requires information about the elastic deformation of tooth surfaces and the principal curvatures and the principal directions of tooth surfaces at each instantaneous point of their tangency.

It will be shown later (Section 1.5) that the path of contact on gear tooth surface is oriented longitudinally. Such a path of contact is favorable for increasing the contact ratio (of the average number of teeth that are in contact simultaneously), allows edge contact to be avoided and improves the conditions of transfer of meshing wherein one pair of teeth is changed for the neighboring one.

The TCA (Tooth Contact Analysis) computer program developed by the authors allows simulation of meshing of surfaces and investigation of the shift of bearing contact caused by errors of alignment. In some cases of design, it may become necessary to adjust the bearing contact – to deviate it from the longitudinal direction – to reduce the shift of bearing contact caused by misalignments.

Application of Parabolic Profiles of Blades of Gear Head-Cutter. We have mentioned above that the gear tooth surface is generated as the copy of the surface of the gear head-cutter. Usually, straight profile blades are applied for the gear head-cutter. Such blades form the head-cutter generating surface as a cone.

Application of parabolic profiles of the blades instead of straight line profiles enables to modify the gear tooth surface in favor of conjugation of pinion-gear tooth surfaces.

Simulation of Meshing. The algorithm of computerized simulation of meshing provides continuous tangency of contacting gear tooth surfaces Σ_1 and Σ_2 as the equality of position vectors $\mathbf{r}_h^{(1)} = \mathbf{r}_h^{(2)}$ and unit normals $\mathbf{n}_h^{(1)} = \mathbf{n}_h^{(2)}$ (see details in Section 1.8). Instead of equality of unit normals to contacting surfaces, collinearity of surface normals may be considered. Position vectors $\mathbf{r}_h^{(i)}(i = 1,2)$ and unit normals $\mathbf{n}_h^{(i)}(i = 1,2)$ are considered in fixed coordinate system S_h (Fig. 1.1).
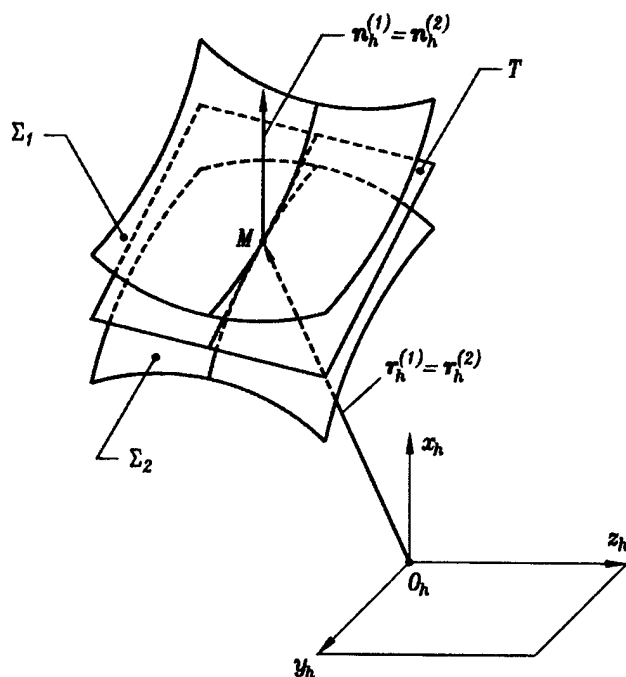

Figure 1.1: Illustration of tangency of surfaces Σ_1 and Σ_2.

Application of TCA permits the determination of the paths of contact on pinion-gear tooth surfaces, dimensions and orientation of instantaneous contact ellipse at each point of contact, the transmission function $\phi_2(\phi_1)$ that relates the angles of rotation of the gear and the pinion, and function $\Delta\phi_2(\phi_1)$ of transmission errors that is determined as

$$\Delta\phi_2(\phi_1) = \phi_2(\phi_1) - \frac{N_1}{N_2}\phi_1 \qquad (1.1)$$

where N_1 and N_2 are the numbers of teeth of the pinion and the gear.

Predesign of Parabolic Function of Transmission Errors. The output of TCA for a misaligned gear drive shows that the transmission function $\phi_2(\phi_1)$ is a piecewise discontinuous almost linear function (Fig. 1.2(a)). The transfer of

meshing with the transmission function $\phi_2(\phi_1)$ (Fig. 1.2(a)) and function $\Delta\phi_2(\phi_1)$ of transmission errors (Fig. 1.2(b)) is accompanied with the jump of the angular velocity ω_2 and therefore noise and vibration are inevitable.
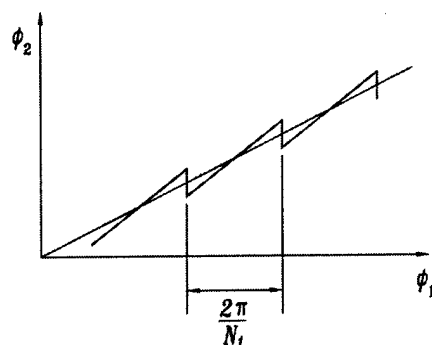
(a)
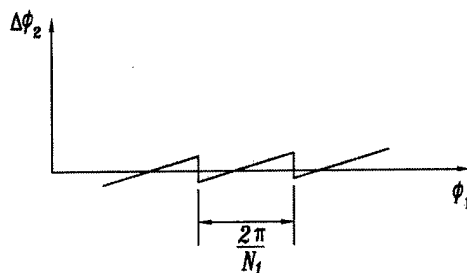
(b)

Figure 1.2: Transmission function (a) and function of transmission errors (b) of a misaligned gear drive.

The purpose of synthesis of low-noise gear drives is to transform the transmission function $\phi_2(\phi_1)$ as shown in Fig. 1.3(a) and obtain a parabolic function of transmission errors shown in Fig. 1.3(b). The modified function $\Delta\phi_2(\phi_1)$ (Fig. 1.3(b)) is a continuous one and is determined as

$$\Delta\phi_2^{(1)}(\phi_1) = -a\phi_1^2 \qquad (1.2)$$

where a is the parabola coefficient.

It is important to recognize that the function of transmission errors must be negative and therefore the gear will lag with respect to the pinion. Therefore, the transfer of meshing is accompanied with elastic deformations, and as a result, the gear ratio is increased.

The desired parabolic function of transmission errors is provided by the respective synthesis of the gear drive. The idea of such a synthesis is based on the predesign of a parabolic function obtained by application of modified roll during the process of generation. Modified roll is provided due to application of nonlinear relations between the angles of rotation of the cradle of the generation machine and the pinion during the process of pinion generation (see Section 1.5).

The advantage of the predesign of a parabolic function of transmission errors is the absorption by such a function of the linear discontinuous function of transmission errors caused by misalignment. This is illustrated by drawings of Fig. 1.4(a) that shows a linear function $\Delta\phi_2^{(2)}(\phi_1) = b\phi_1$ (Fig. 1.4(a)). Parabolic function $\Delta\phi_2^{(1)}(\phi_1)$ is predesigned and linear function $\Delta\phi_2^{(2)}(\phi_1)$ is caused by misalignment. The sum of functions $\Delta\phi_2^{(1)}(\phi_1)$ and $\Delta\phi_2^{(2)}(\phi_1)$ is obtained as a parabolic function and represented in Fig. 1.4(a) as function $\Delta\psi_2(\psi_1) = -a\psi_1^2$. The parabola coefficient a is the same in functions $\Delta\phi_2^{(1)}(\phi_1)$ and $\Delta\psi_2(\psi_1)$.
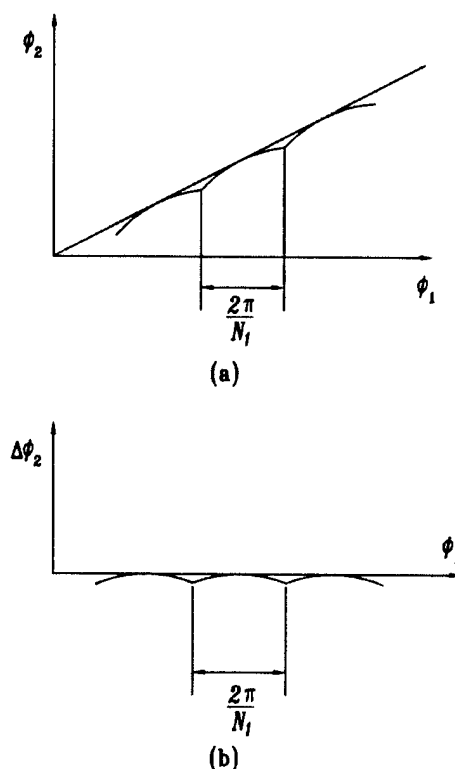
Figure 1.3: Transmission function (a) and function of transmission errors
(b) of a gear drive with a predesigned parabolic function.

The drawings confirm: (i) the predesigned parabolic function absorbs indeed linear function $\Delta\phi_2^{(2)}(\phi_1)$, and (ii) the resulting function $\Delta\psi_2(\psi_1)$ is slightly dislocated with respect to origin of $\Delta\phi_2^{(1)}(\phi_1)$, function $\Delta\psi_2(\psi_1)$ is an asymmetrical one. Parameters c and d of the origin of $\Delta\psi_2(\psi_1)$ are determined as $d = b^2/4a$, $c = b/2a$. In the process of meshing, wherein several cycles of meshing are considered (Fig. 1.4(b)), the resulting function $\Delta\psi_2(\psi_1)$ of transmission errors becomes a symmetric parabolic function.

The authors have developed computerized synthesis of formate-cut spiral bevel gears that is based on simultaneous application of local synthesis and simulation of meshing and contact of gear tooth surfaces.

The purpose of local synthesis is determination of the pinion machine-tool settings considering as given: (i) the gear machine-tool settings, and (ii) the conditions of meshing and contact at the mean contact point M such as the tangent to the path of contact at M, the major axis of the contact ellipse at M, and the derivative of the function of transmission errors.

The purpose of simulation of meshing and contact is the determination of the bearing contact and function of transmission errors knowing the pinion and gear machine-tool settings.

The applied computational procedures are iterative processes (see Section 1.5) with the goals to obtain: (i) a longitudinally directed bearing contact, (ii) a parabolic function of transmission errors with limited value of maximal errors, and (iii) reduced sensitivity of the gear drive to errors of alignment.
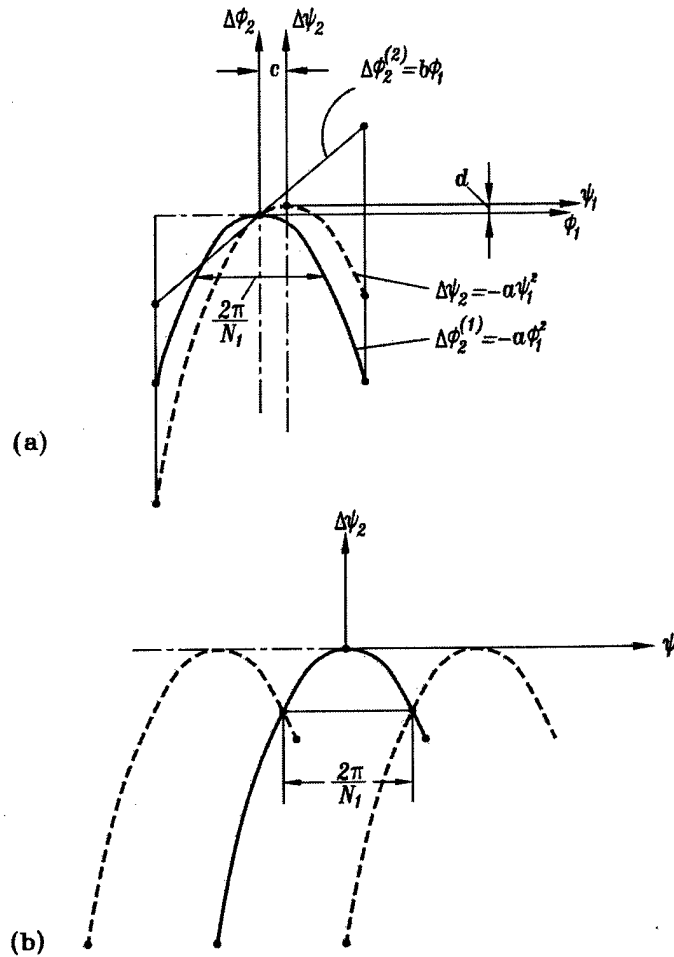
Figure 1.4: Interaction of predesigned parabolic function $\Delta\phi_2^{(1)}(\phi_1)$ with linear function $\Delta\phi_2^{(2)}(\phi_1)$ caused by misalignment.

1.3 Derivation of Gear Tooth Surface

Applied Coordinate Systems. Coordinate system S_{m_2} is the fixed one and it is rigidly connected to the cutting machine (Fig. 1.5). Figure 1.5(a) and (b) show two sets of coordinate systems applied for generation of left- and right-hand gears, respectively. Coordinate system S_2 is rigidly connected to the gear. Coordinate system S_g is rigidly connected to the gear head-cutter. It is considered that the gear head-cutter is a surface of revolution, and the rotation of the head cutter about the x_g axis does not affect the process of generation.

The installment of the tool on the machine is determined by parameters H_2 and V_2, that are called horizontal and vertical settings. Parameters X_G and γ_{m_2} represent the settings of the gear.
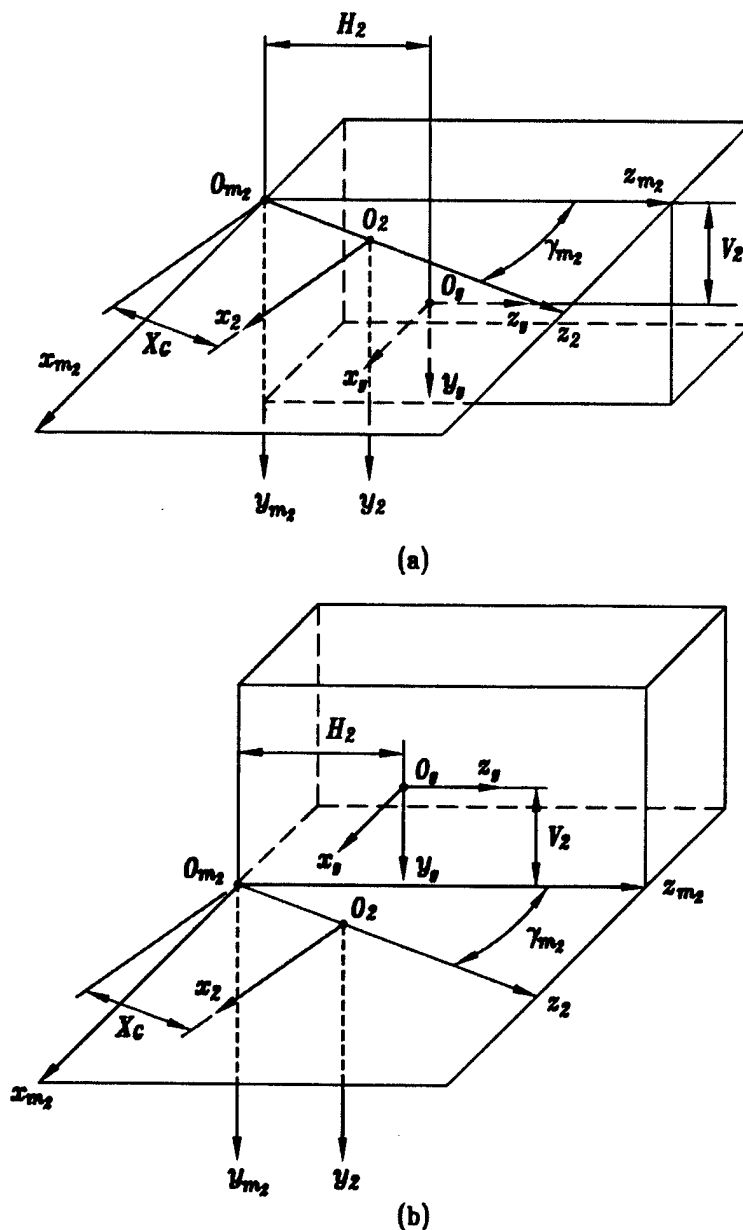
(a)

(b)

Figure 1.5: Machine tool settings for gear generation: (a) for left-hand gear and (b) for right-hand gear.

Head Cutter Surface. Blades of parabolic profile (Fig. 1.6(a)) are applied for the gear head-cutter. Each side of the blade generates two sub-surfaces. The segment a of the parabolic profile generates the working part of the gear tooth surface. The circular arc of radius ρ_w generates the fillet of the gear tooth surface. The generating surfaces of the head cutter are formed by rotation of the blade about the x_g axis of the head-cutter (Figs. 1.6(b) and (c)); the rotation angle is θ_g. Therefore, the generating surfaces are: (i) surface of revolution formed by rotation of the blade of parabolic profile (part a), and (ii) the surface of the torus formed by rotation of the circular arc profiles (part b). A point on the generating surface is determined by parameters u_g and θ_g for the working surface, and by λ_w and θ_g for the fillet surface. Angle α_g is formed between the tangent line of the blade at point M and the vertical centerline of the blade.

Parameter u_g measured from point M in the chosen direction is considered as a positive one, and angles α_g and λ_w as the acute ones. The apex of the parabola is located at point M determined by parameter s_{g_0}.
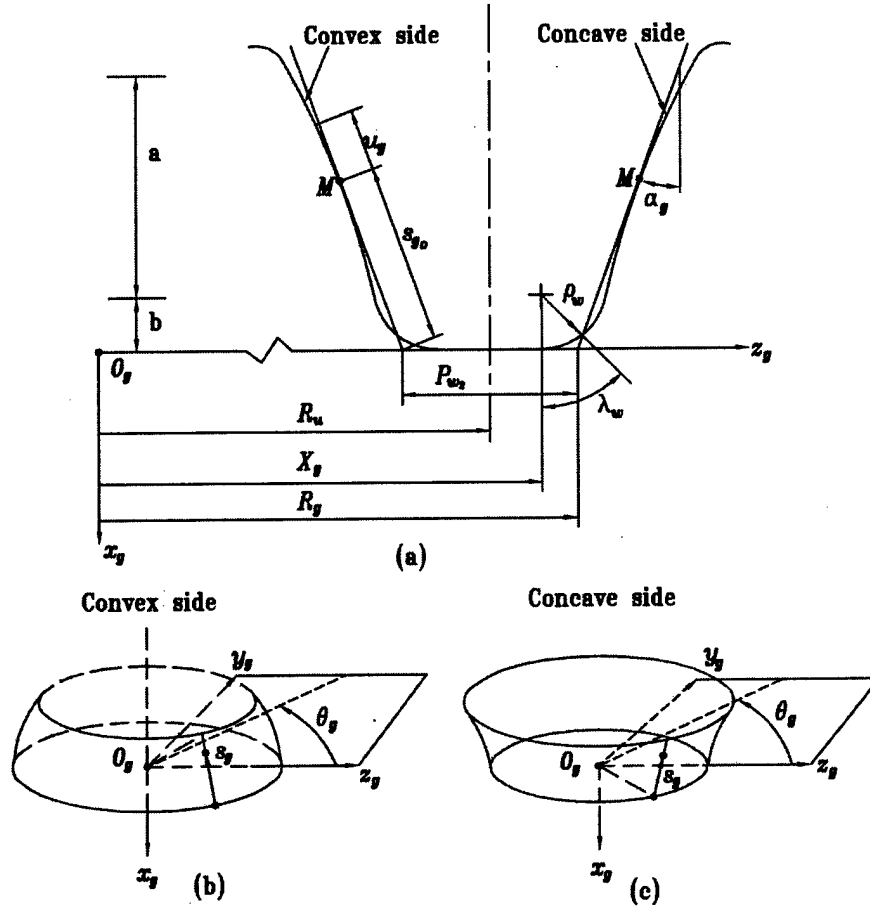
Figure 1.6: Illustration of gear cutter blades and generating surfaces.

The surface of revolution and the torus surface of the head-cutter are designated as parts a and b of the head-cutter generating surface. Surface $\Sigma_g^{(a)}$ of the head-cutter is represented by vector function $\mathbf{r}_g^{(a)}(u_g,\theta_g)$ as follows

$$\mathbf{r}_g^{(a)}(u_g,\theta_g) = \begin{bmatrix} -u_g\cos\alpha_g + a_c u_g^2\sin\alpha_g - s_{g_0}\cos\alpha_g \\ (R_g \pm s_{g_0}\sin\alpha_g \pm u_g\sin\alpha_g \pm a_c u_g^2\cos\alpha_g)\sin\theta_g \\ (R_g \pm s_{g_0}\sin\alpha_g \pm u_g\sin\alpha_g \pm a_c u_g^2\cos\alpha_g)\cos\theta_g \end{bmatrix} \tag{1.3}$$

where u_g and θ_g are the surface coordinates, α_g is the blade angle at point M, R_g is the cutter point radius (Fig. 1.6) and given by

$$R_g = R_u \pm \frac{P_{w_2}}{2} \tag{1.4}$$

The upper and lower signs in equations (1.3) and (1.4) correspond to the concave and convex sides of the gear tooth, respectively.

The unit normal to the gear generating surface $\Sigma_g^{(a)}$ is represented by the equations

$$\mathbf{n}_g^{(a)}(u_g,\theta_g)=\frac{\mathbf{N}_g^{(a)}}{\left|\mathbf{N}_g^{(a)}\right|},\qquad \mathbf{N}_g^{(a)}=\frac{\partial\mathbf{r}_g^{(a)}}{\partial u_g}\times\frac{\partial\mathbf{r}_g^{(a)}}{\partial\theta_g}\tag{1.5}$$

Equations (1.3) and (1.5) yield

$$\mathbf{n}_g^{(a)}(u_g,\theta_g)=\begin{bmatrix}\pm\sin\alpha_g\pm 2a_cu_g\cos\alpha_g\\(\cos\alpha_g-2a_cu_g\sin\alpha_g)\sin\theta_g\\(\cos\alpha_g-2a_cu_g\sin\alpha_g)\cos\theta_g\end{bmatrix}\div\sqrt{1+4a_c^2u_g^2}\tag{1.6}$$

Surface $\Sigma_g^{(b)}$ is represented in S_g as

$$\mathbf{r}_g^{(b)}(\lambda_w,\theta_g)=\begin{bmatrix}-\rho_w(1-\cos\lambda_w)\\(X_g\pm\rho_w\sin\lambda_w)\sin\theta_g\\(X_g\pm\rho_w\sin\lambda_w)\cos\theta_g\end{bmatrix}\tag{1.7}$$

where

$$(X_g=R_g\mp\rho_w(1-\sin\alpha_g)/\cos\alpha_g$$

Here, ρ_w is the fillet radius of the gear generating surface.

The unit normal to the gear generating surface $\Sigma_g^{(b)}$ is represented by the equations

$$\mathbf{n}_g^{(b)}(\lambda_w,\theta_g)=\frac{\mathbf{N}_g^{(b)}}{\left|\mathbf{N}_g^{(b)}\right|},\qquad \mathbf{N}_g^{(b)}=\frac{\partial\mathbf{r}_g^{(b)}}{\partial\lambda_w}\times\frac{\partial\mathbf{r}_g^{(b)}}{\partial\theta_g}\tag{1.8}$$

Equations (1.8) yield

$$\mathbf{n}_g^{(b)}(\lambda_w,\theta_g)=\begin{bmatrix}\pm\cos\lambda_w\\\sin\lambda_w\sin\theta_g\\\sin\lambda_w\cos\theta_g\end{bmatrix}\tag{1.9}$$

Equations of Head-Cutter Surfaces in S_2. Applying coordinate transformation from S_g to S_2, the gear tooth surfaces can be represented in S_2 by the equations

$$\mathbf{r}_2^{(a)}(u_g,\theta_g)=\mathbf{M}_{2g}\mathbf{r}_g^{(a)}(u_g,\theta_g)\tag{1.10}$$

$$\mathbf{r}_2^{(b)}(\lambda_w,\theta_g)=\mathbf{M}_{2g}\mathbf{r}_g^{(a)}(\lambda_w,\theta_g)\tag{1.11}$$

Here

$$\mathbf{M}_{2g}=\mathbf{M}_{2m_2}\mathbf{M}_{m_2g}\tag{1.12}$$

$$\mathbf{M}_{m_2g}=\begin{bmatrix}1&0&0&0\\0&1&0&\pm V_2\\0&0&1&H_2\\0&0&0&1\end{bmatrix}$$

$$\mathbf{M}_{2m_2}=\begin{bmatrix}\cos\gamma_{m_2}&0&-\sin\gamma_{m_2}&0\\0&1&0&0\\\sin\gamma_{m_2}&0&\cos\gamma_{m_2}&-X_G\\0&0&0&1\end{bmatrix}$$

Here V_2, H_2, and X_G (Fig. 1.5) are the gear machine tool settings. The upper and lower signs in front of V_2 correspond to right-hand and left-hand gears, respectively. The whole set of gear machine tool settings is represented in Table 1. We remind that the generated gear tooth surface is a copy of the surface of the head-cutter, that is a surface of revolution. The rotation of the head-cutter about the x_g axis is necessary for the cutting or grinding process but does not affect the shape of gear tooth surfaces.

Table 1.1: Gear machine tool settings.

Blade angle α_g (Fig. 1.6)
Blade parabolic coefficient a_c
Parabola apex location s_{g_0}
Cutter (grinding wheel) radius R_u (mm) (Fig. 1.6)
Point width P_{w_2} (mm) (Fig. 1.6)
Cutter point radius R_g (mm) (Fig. 1.6) ($R_g = R_u \pm P_{w_2}/2$)
Horizontal setting H_2 (mm) (Fig. 1.5)
Vertical setting V_2 (mm) (Fig. 1.5)
Machine center to back X_G (mm) (Fig. 1.5)
Machine root angle γ_{m_2} (Fig. 1.5)
Fillet radius ρ_w (mm) (Fig. 1.6)

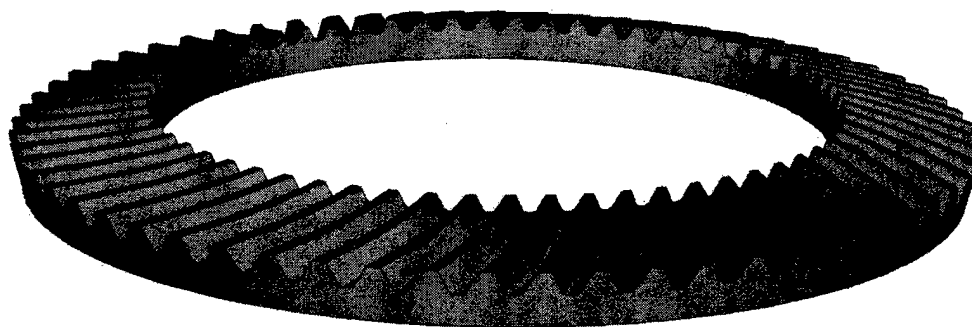A 3D geometric model of the gear tooth surfaces is shown in Fig. 1.7.

Figure 1.7: 3D geometric model of gear tooth surfaces.

1.4 Derivation of Pinion Tooth Surface

Applied Coordinate Systems. Coordinate systems applied for generation of pinion are shown in Figs. 1.8 and 1.9. Figures 1.9(a) and (b) correspond to generation of right- and left-hand pinions, respectively. Coordinate systems S_{m_1}, S_{a_1}, S_{b_1} are the fixed ones and they are rigidly connected to the cutting machine. The movable coordinate systems S_1 and S_{c_1} are rigidly connected to the pinion and the cradle, respectively. The coordinate systems S_1 and S_{c_1} are rotated about the z_{m_1} axis and z_{b_1} axis, respectively, and the angles of rotation are related by a polynomial function $\psi_1(\psi_{c_1})$ if modified roll is applied (see below). The ratio of instantaneous angular velocities of the pinion and the cradle is defined as $m_{1c}(\psi_1(\psi_{c_1})) = \omega^{(1)}(\psi_{c_1})/\omega^{(c)}$. The magnitude $m_{1c}(\psi_1)$ at ψ_{c_1} is called ratio of roll. Parameters X_{D_1}, X_{B_1}, E_{m_1}, and γ_{m_1} are the basic machine tool settings for pinion generation.
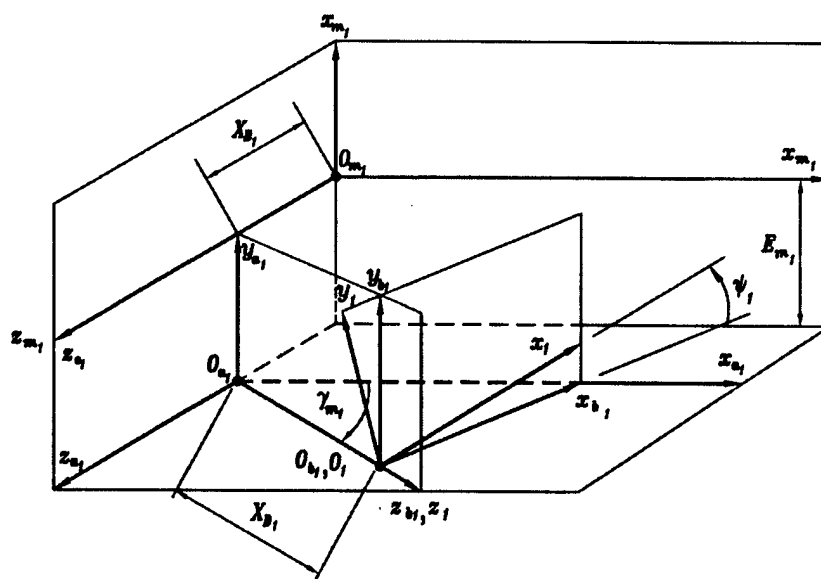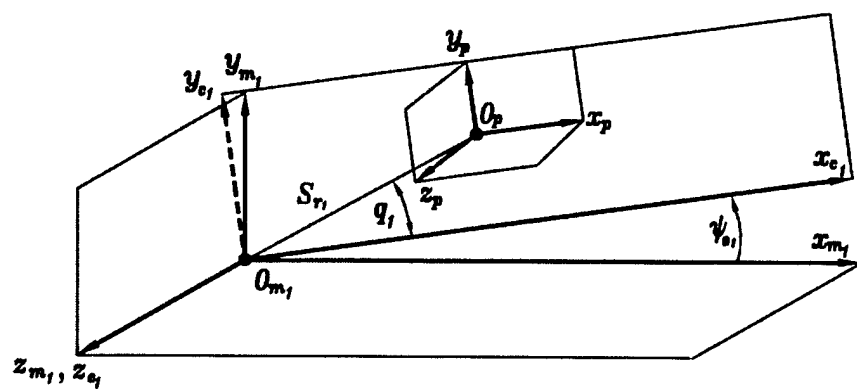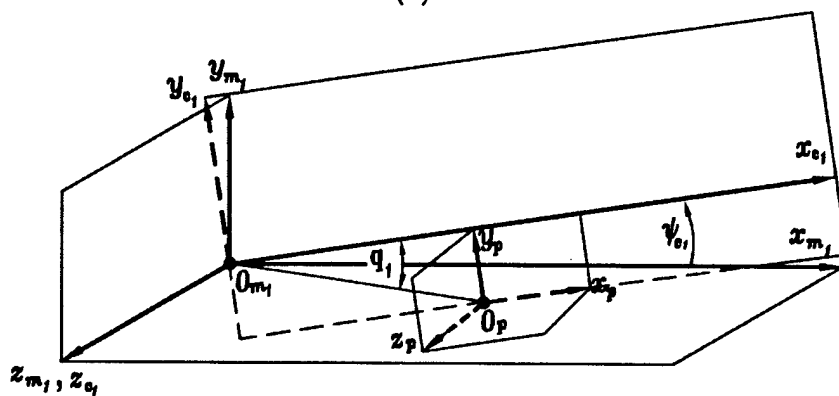
Figure 1.8: Machine tool settings for installment of the to-be-generated pinion.

(a)

(b)

Figure 1.9: Machine tool settings for installment of pinion head-cutter:
(a) for right-hand pinion; (b) for left-hand pinion.

Head Cutter Surfaces. The pinion generating surfaces are formed by surface $\Sigma_p^{(a)}$ and $\Sigma_p^{(b)}$ generated by straight-line and circular arc parts of the blades (Fig. 1.10). Surface $\Sigma_p^{(a)}$ is represented as

$$\mathbf{r}_p^{(a)}(s_p, \theta_p) = \begin{bmatrix} (R_p \mp s_p \sin\alpha_p)\cos\theta_p \\ (R_p \mp s_p \sin\alpha_p)\sin\theta_p \\ -s_p \cos\alpha_p \end{bmatrix} \tag{1.13}$$

where s_p and θ_p are the surface coordinates; α_p is the blade angle; R_p is the cutter point radius (Fig. 1.10). The upper and lower signs in equations (1.13) correspond to the convex and concave sides of the pinion tooth respectively.
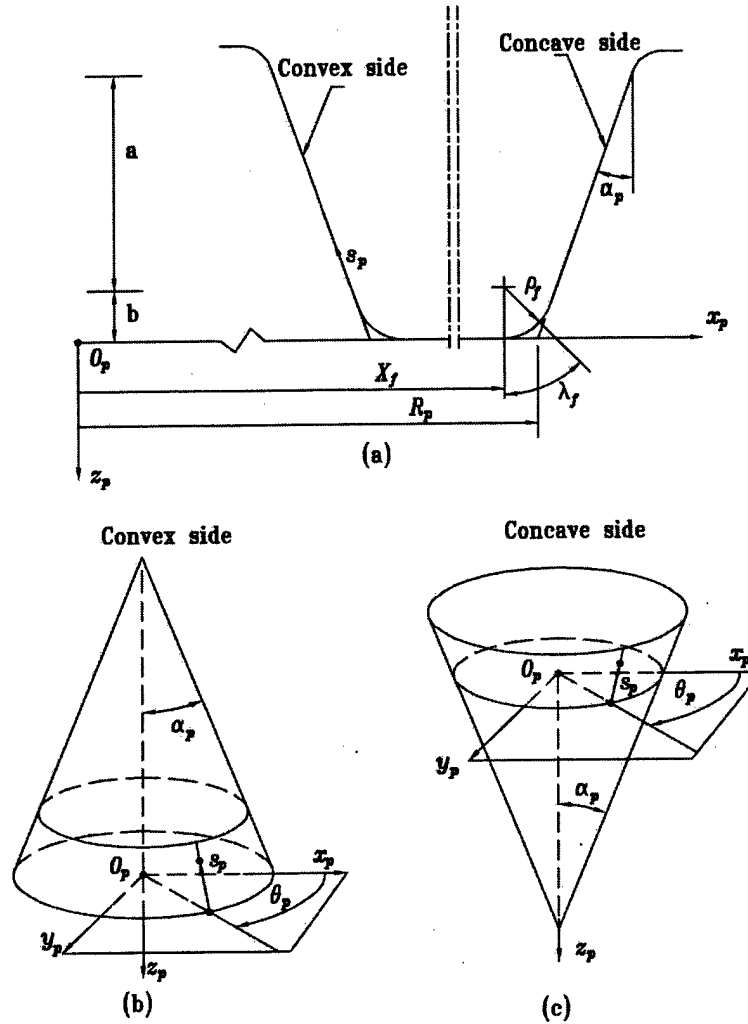

Figure 1.10: Illustration of pinion cutter blades and generating surfaces.

The unit normal to the pinion generating surface $\Sigma_p^{(a)}$ is represented by the equations

$$\mathbf{n}_p^{(a)}(\theta_p) = \frac{\mathbf{N}_p^{(a)}}{\left|\mathbf{N}_p^{(a)}\right|}, \qquad \mathbf{N}_p^{(a)} = \frac{\partial \mathbf{r}_p^{(a)}}{\partial s_p} \times \frac{\partial \mathbf{r}_p^{(a)}}{\partial \theta_p} \tag{1.14}$$

Equations (1.13) and (1.14) yield

$$\mathbf{n}_p^{(a)}(\theta_p) = \begin{bmatrix} \cos\alpha_p \cos\theta_p \\ \cos\alpha_p \sin\theta_p \\ \mp\sin\alpha_p \end{bmatrix} \tag{1.15}$$

For the fillet surface $\Sigma_p^{(b)}$, we obtain

$$\mathbf{r}_p^{(b)}(\lambda_f,\theta_p) = \begin{bmatrix} (X_f \mp \rho_f \sin\lambda_f)\cos\theta_p \\ (X_f \mp \rho_f \sin\lambda_f)\sin\theta_p \\ -\rho_f(1-\cos\lambda_f) \end{bmatrix} \tag{1.16}$$

where

$$X_f = R_p \pm \rho_f(1-\sin\alpha_f)/\cos\alpha_f$$

and ρ_f is the radius of the tool fillet.

The unit normal to the pinion generating surface of part b is represented by the equations

$$\mathbf{n}_p^{(b)}(\lambda_f,\theta_p) = \frac{\mathbf{N}_p^{(b)}}{\left|\mathbf{N}_p^{(b)}\right|}, \qquad \mathbf{N}_p^{(b)} = \frac{\partial \mathbf{r}_p^{(b)}}{\partial\lambda_f} \times \frac{\partial \mathbf{r}_p^{(b)}}{\partial\theta_p} \tag{1.17}$$

Equations (1.17) yield

$$\mathbf{n}_p^{(b)}(\lambda_f,\theta_p) = \begin{bmatrix} \sin\lambda_f \cos\theta_p \\ \sin\lambda_f \sin\theta_p \\ \mp\cos\lambda_f \end{bmatrix} \tag{1.18}$$

The head-cutter is mounted on coordinate system S_{c_1} (called the cradle of the cutting machine) and its installments are determined by settings S_{r_1} and q_1 (Fig. 1.9). In the process for pinion generation, coordinate systems S_{c_1} and S_1 perform related rotations with respect to S_{m_1}. Then, a family of pinion head-cutter surfaces is generated in coordinate system S_1 determined as

$$\mathbf{r}_1^{(a)}(s_p,\theta_p,\psi_1) = \mathbf{M}_{1p}(\psi_1)\mathbf{r}_p^{(a)}(s_p,\theta_p) \tag{1.19}$$

$$\mathbf{r}_1^{(b)}(\lambda_f,\theta_p,\psi_1) = \mathbf{M}_{1p}(\psi_1)\mathbf{r}_p^{(b)}(\lambda_f,\theta_p) \tag{1.20}$$

Here ψ_1 is the generalized parameter of motion, and the used matrices are determined as

$$\mathbf{M}_{1p} = \mathbf{M}_{1b_1}\mathbf{M}_{b_1a_1}\mathbf{M}_{a_1m_1}\mathbf{M}_{m_1c_1}\mathbf{M}_{c_1p}$$

$$\mathbf{M}_{c_1p} = \begin{bmatrix} 1 & 0 & 0 & S_{r_1}\cos q_1 \\ 0 & 1 & 0 & \pm S_{r_1}\sin q_1 \\ 0 & 0 & 1 & 0 \\ 0 & 0 & 0 & 1 \end{bmatrix}$$

$$\mathbf{M}_{m_1c_1} = \begin{bmatrix} \cos\psi_{c1} & -\sin\psi_{c1} & 0 & 0 \\ \sin\psi_{c1} & \cos\psi_{c1} & 0 & 0 \\ 0 & 0 & 1 & 0 \\ 0 & 0 & 0 & 1 \end{bmatrix}$$

$$\mathbf{M}_{a_1m_1} = \begin{bmatrix} 1 & 0 & 0 & 0 \\ 0 & 1 & 0 & E_{m1} \\ 0 & 0 & 1 & -X_{B_1} \\ 0 & 0 & 0 & 1 \end{bmatrix}$$

$$\mathbf{M}_{b_1 a_1} = \begin{bmatrix} \sin\gamma_{m_1} & 0 & -\cos\gamma_{m_1} & 0 \\ 0 & 1 & 0 & 0 \\ \cos\gamma_{m_1} & 0 & \sin\gamma_{m_1} & -X_{D_1} \\ 0 & 0 & 0 & 1 \end{bmatrix}$$

$$\mathbf{M}_{1b_1} = \begin{bmatrix} \cos\psi_1 & \sin\psi_1 & 0 & 0 \\ -\sin\psi_1 & \cos\psi_1 & 0 & 0 \\ 0 & 0 & 1 & 0 \\ 0 & 0 & 0 & 1 \end{bmatrix}$$

The upper and lower signs of the element $S_{r_1} \sin q_1$ in matrix $\mathbf{M}_{c_1 p}$ correspond to generation of right- and left-hand pinions, respectively. Wherein the modified roll is applied in the process of generation, the rotation angles ψ_1 and ψ_{c_1} of the pinion and cradle are related as

$$\psi_1 = b_1 \psi_{c_1} - b_2 \psi_{c_1}^2 - b_3 \psi_{c_1}^3 = b_1 \left(\psi_{c_1} - \frac{b_2}{b_1} \psi_{c_1}^2 - \frac{b_3}{b_1} \psi_{c_1}^3 \right) = m_{1c} \left(\psi_{c_1} - C\psi_{c_1}^2 - D\psi_{c_1}^3 \right) \tag{1.21}$$

where b_2 and b_3 are the modified roll parameters and C and D the modified roll coefficients.

The derivative of function $\psi_1(\psi_{c_1})$ taken at $\psi_{c_1} = 0$ determines the so-called ratio of roll represented in equation (1.21) by b_1 or m_{1c}.

Equation of Meshing. The pinion tooth surface Σ_1 is the envelope to the family of head-cutter surfaces. Surface Σ_1 consists of two surfaces that correspond to the cutter surfaces $\Sigma_p^{(a)}$ and $\Sigma_p^{(b)}$, respectively. The modified roll is applied in the process of generation. The equation of meshing for generation of surface $\Sigma_p^{(a)}$ is represented as

$$\mathbf{n}_{m_1}^{(a)} \cdot \mathbf{v}_{m_1}^{(p1)} = f_{1p}^{(a)}(s_p, \theta_p, \psi_1) = 0 \tag{1.22}$$

where $\mathbf{n}_{m_1}^{(a)}$ is the unit normal to the surface, and $\mathbf{v}_{m_1}^{(p1)}$ is the velocity in relative motion. These vectors are represented in the fixed coordinate system S_{m_1} as follows:

$$\mathbf{n}_{m_1}^{(a)} = \mathbf{L}_{m_1 c_1} \mathbf{L}_{c_1 p} \mathbf{n}_p^{(a)}(\theta_p) \tag{1.23}$$

$$\mathbf{v}_{m_1}^{(p1)} = \left[\left(\boldsymbol{\omega}_{m_1}^{(p)} - \boldsymbol{\omega}_{m_1}^{(1)} \right) \times \mathbf{r}_{m_1} \right] - \left(\overline{O_{m_1} O_{a_1}} \times \boldsymbol{\omega}_{m_1}^{(1)} \right) \tag{1.24}$$

Here

$$\mathbf{r}_{m_1} = \mathbf{M}_{m_1 c_1} \mathbf{M}_{c_1 p} \mathbf{r}_p^{(a)}(s_p, \theta_p)$$

$$\overline{O_{m_1} O_{a_1}} = \begin{bmatrix} 0 & -E_{m_1} & X_{B_1} \end{bmatrix}^T$$

$$\boldsymbol{\omega}_{m1}^{(1)} = \begin{bmatrix} \cos\gamma_{m_1} & 0 & \sin\gamma_{m_1} \end{bmatrix}^T$$

$$\boldsymbol{\omega}_{m1}^{(p)} = \begin{bmatrix} 0 & 0 & m_{c1}(\psi_{c1}) \end{bmatrix}^T$$

The ratio m_{c1} is not constant since modified roll is applied and can be represented as

$$m_{c1}\circ(\psi_{c_1}) = \frac{\omega_{c1}}{\omega_1} = \frac{d\psi_{c1}}{dt} \Big/ \frac{d\psi_1}{dt} = \frac{1}{m_{1c}\left(1 - 2C\psi_{c1} - 3D\psi_{c1}^2\right)} = \frac{1}{m_{1c} - 2b_2\psi_{c1} - 3b_3\psi_{c1}^2} \tag{1.25}$$

where C and D are modified roll coefficients.

Finally, we obtain the equations for pinion tooth surface $\Sigma_p^{(a)}$ as

$$\mathbf{r}_1^{(a)}(s_p, \theta_p, \psi_1) = \mathbf{M}_{1p}(\psi_1) \mathbf{r}_p^{(a)}(s_p, \theta_p) \tag{1.26}$$

$$f_{1p}^{(a)}(s_p, \theta_p, \psi_1) = 0 \tag{1.27}$$

Similarly, the pinion fillet surface $\Sigma_p^{(b)}$ may be represented as

$$\mathbf{r}_1^{(b)}(\lambda_f, \theta_p, \psi_1) = \mathbf{M}_{1p}(\psi_1)\mathbf{r}_p^{(b)}(\lambda_f, \theta_p) \qquad (1.28)$$

$$f_{1p}^{(b)}(\lambda_f, \theta_p, \psi_1) = 0 \qquad (1.29)$$

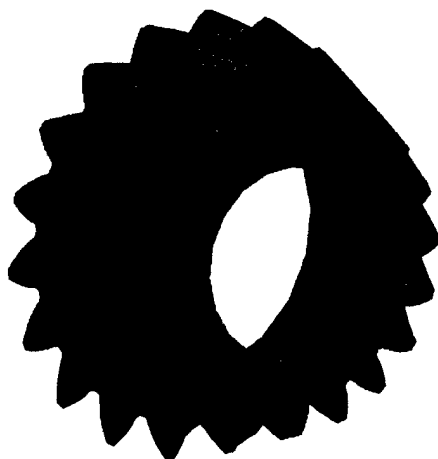The geometric model of pinion tooth surfaces is shown in Fig. 1.11.

Figure 1.11: 3D geometric model of pinion tooth surfaces.

1.5 Procedures of Proposed Design

The authors have developed an approach for the design of formate cut spiral bevel gears that provides a stabilized bearing contact and reduced level of noise.

The bearing contact is of a longitudinal direction that permits an increase in the contact ratio, avoids edge contact, and reduces the shift of the bearing contact caused by misalignment.

The reduction of noise is achieved by application of a predesigned parabolic function and limitation of maximal transmission errors caused by misalignment.

The approach is based on four procedures that require simultaneous application of the computational algorithms developed for local synthesis and simulation of meshing and contact of the gear drive.

The purpose of the local synthesis is to determine the pinion machine-tool settings for the following conditions of meshing and contact of pinion-gear tooth surfaces Σ_1 and Σ_2 :

(i)   The gear machine-tool settings are considered as given (they may be adapted, for instance, from a Gleason summary for gear generation).

(ii)   The pinion-gear tooth surfaces Σ_1 and Σ_2 are in tangency at a chosen mean contact point M (Fig. 1.12).

(iii)   Parameters $2a$, η_2, and m'_{12} are preassigned and determine the conditions of meshing and contact of Σ_1 and Σ_2 at point M and in the neighborhood at M. Here, $2a$ is the major axis of the instantaneous contact ellipse, η_2 determines the tangent to the path of contact on the gear tooth surface at M, and m'_{12} is the derivative $\partial m_{12}(\phi_1)/\partial \phi_1$ at point M where $m_{12}(\phi_1)$ is the gear ratio.

Note: It will be shown in Section 1.6 that the location of point M_2 on the gear tooth surface, as the candidate for the mean contact point of Σ_1 and Σ_2, may be chosen ahead. Then, the procedure of the local synthesis permits determining such a point M_1 on pinion tooth surface Σ_1 that will be in tangency with Σ_2 at the chosen point M_2 of Σ_2.
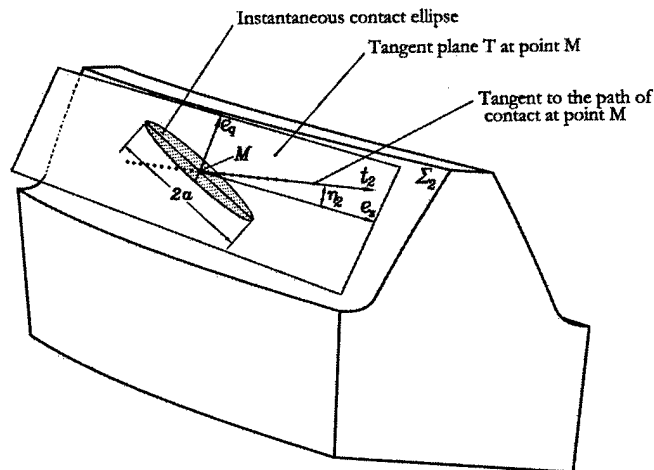
Figure 1.12: Illustration of parameters η_2 and a applied for local synthesis.

The simulation of meshing and contact of pinion-gear tooth surfaces is accomplished by application of the developed TCA (Tooth Contact Analysis) computer program. The inputs for TCA are the equations of pinion-gear tooth surfaces, parameters of motion and assembly. The outputs are the bearing contact and the function of transmission errors.

The design is based on simultaneous application of the computational algorithms developed for local synthesis and TCA, it is an iterative process, and requires application of the following four procedures:

Procedure 1: The path of contact on gear tooth surface is a spatial curve L. Projection of L on tangent plane T (Fig. 1.13) is designated by L_T. The purpose of procedure 1 is to obtain L_T that is a straight line directed longitudinally. Figure 1.13 shows projections $L_T^{(1)}$ and $L_T^{(2)}$ that deviate from the desired line L_T.
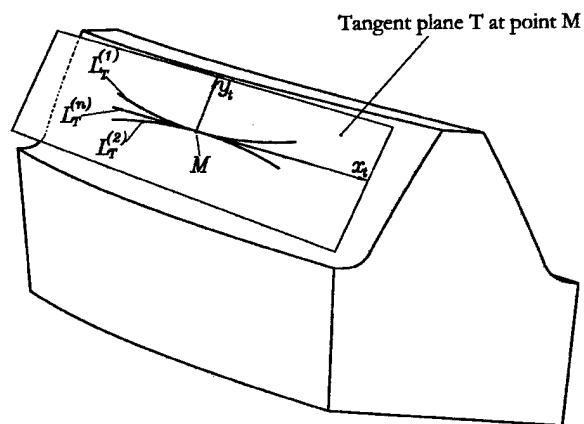

Figure 1.13: Projections of various paths of contact L_T on tangent plane T.

Figure 1.14 shows the flow chart that describes the steps of procedure 1. The procedure of computation is an iterative process and requires variation of parameter m'_{12}. The steps of the procedure are as follows:
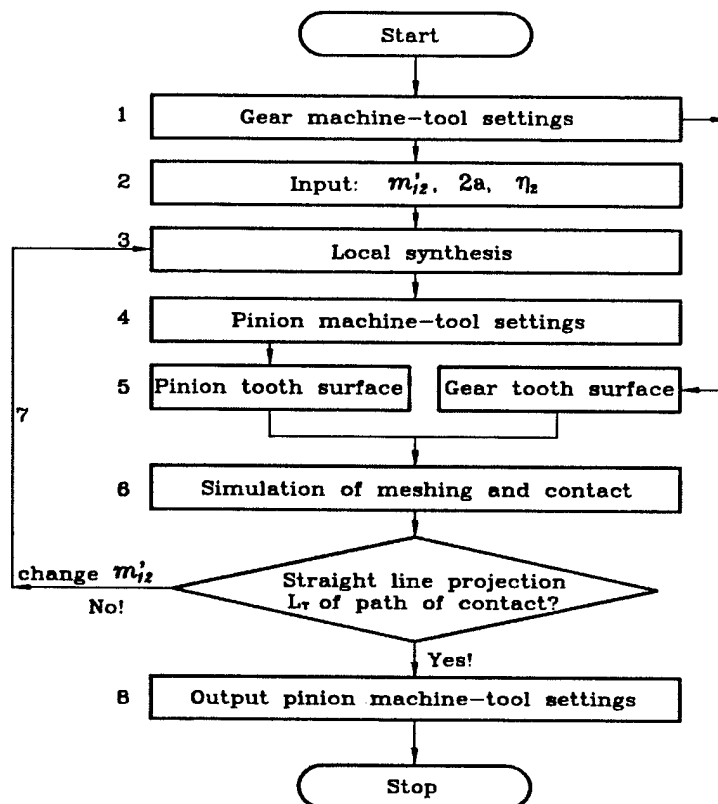

Figure 1.14: Flow chart for procedure 1: design of bearing contact.

Step 1: Input the gear machine-tool settings into the program of local synthesis.

Step 2: Input parameters $2a$, η_2, and m'_{12} into the program of local synthesis.

Step 3: Apply the program of local synthesis.

Step 4: Determine from the computational algorithm of local synthesis the pinion machine-tool settings.

Step 5: Using the machine-tool settings obtained, compute the pinion and gear tooth surfaces Σ_1 and Σ_2.

Step 6: Apply TCA computer program and obtain projection L_T of the path of contact L on tangent plane T (Fig. 1.13).

Step 7: Apply the iterative process and obtain the projection of the path of contact L_T as a straight line by variation of m'_{12}.

Step 8: Obtain as the output the final machine-tool settings for the pinion.

The iterative process is based on the following considerations:

    (i)   The TCA computer program determines the projection L_T of the path of contact numerically.

    (ii)   Consider L_T in coordinate system S_T (Fig. 1.13) with the origin coinciding with M and axes (x_t, y_t) are located in plane T. Axis x_t is the tangent to L_T at point M.

    (iii)   Represent projection L_T as a parabolic regression equation by using a regression subroutine [14]

$$y_t(x_t, m'_{12}) = \beta_o(m'_{12}) + \beta_1(m'_{12})x_t + \beta_2(m'_{12})x_t^2 \qquad (1.30)$$

where $m'_{12} = \partial m_{12}(\phi_1)/\partial\phi_1$ is the input parameter that is varied in the process of iteration.

(iv) The goal is to represent L_T as a straight line that might be obtained by such a magnitude of m'_{12} whereas coefficient $\beta_2(m'_{12}) = 0$ (see Eq. (1.30)). The iterations for determination of $\beta_2(m'_{12}) = 0$ are executed by applying the secant method [13] and illustrated by Fig. 1.15. Equation (1.30) with $\beta_2(m'_{12}) = 0$ provides the projection L_T of path of contact as a straight line.
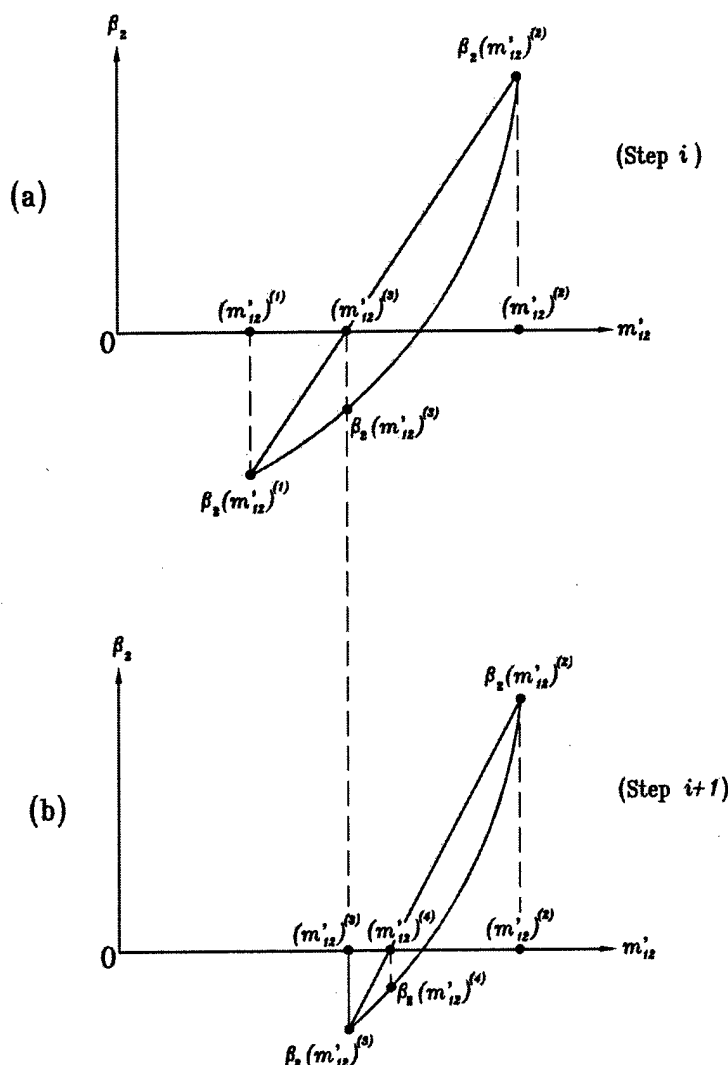

Figure 1.15: Illustration of computations for determination of $\beta_2(m'_{12}) = 0$

Procedure 2: The previously discussed procedure 1 provides the desired longitudinal path of contact and bearing contact. However, the shape of the obtained function of transmission errors and the magnitude of maximal transmission errors do not satisfy the requirements of low-noise gear drive. The goal of procedure 2 is to obtain a parabolic function of negative transmission errors and of limited value of maximal errors.

The sequence of steps applied for procedure 2 is represented by the flow chart shown in Fig. 1.16.

At the start, we use the pinion and gear machine tool settings obtained in procedure 1, but consider that the pinion is generated by application of modified roll. Then, we compute the gear and pinion tooth surfaces Σ_1 and Σ_2, and use

them for the TCA computer program. The intermediate output of TCA is a function of transmission errors. We compare it with the sought-for parabolic function of transmission errors and determine the necessary corrections of modified roll. Repeating the procedure discussed above, we can obtain finally the sought-for parabolic function of transmission errors.
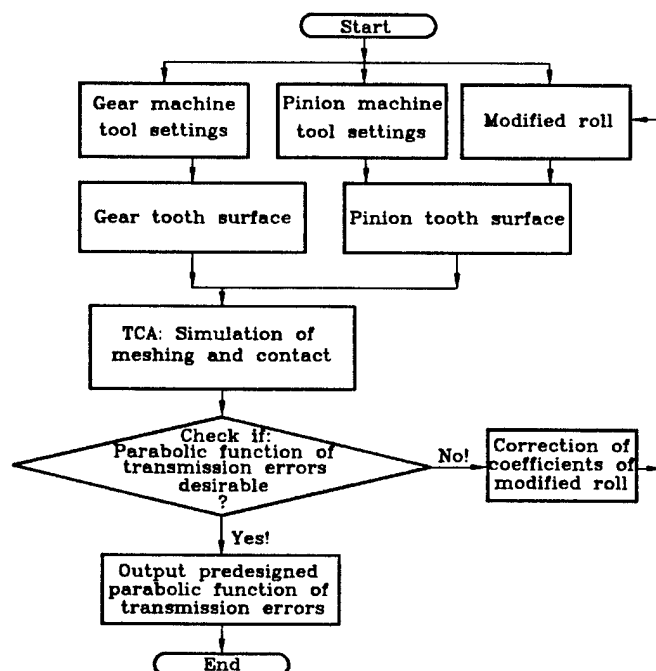

Figure 1.16: Flow chart of procedure 2.

Analytically, the algorithm of procedure 2 is represented as follows.

Step 1: Function of transmission errors $\Delta\phi_2(\phi_1)$ obtained from TCA is numerically represented as a polynomial function up to third member to be included

$$\Delta\phi_2^{(1)}(\phi_1) = a_0 + a_1\phi_1 + a_2\phi_1^2 + a_3\phi_1^3 \tag{1.31}$$

The shape and magnitude of maximal errors of function $\Delta\phi_2^{(1)}(\phi_1)$ do not satisfy the requirements of a low-noise gear drive. Function (1.31) has to be transformed into a parabolic function with limited magnitude of transmission errors by application of procedure 2.

Step 2: We apply for transformation of function $\Delta\phi_2^{(1)}(\phi_1)$ the modified roll for generation of the pinion that is represented as

$$\psi_1(\psi_{c1}) = m_{1c}\psi_{c1} - b_2\psi_{c1}^2 - b_3\psi_{c1}^3 \tag{1.32}$$

Here ψ_1 and ψ_{c1} are the angles of rotation of the pinion and the cradle performed during the process for generation, m_{1c} is the first derivative of $\psi_1(\psi_{c1})$ taken at $\psi_{c1} = 0$ and obtained by the procedure of local synthesis (see Section 1.6). Coefficients b_2 and b_3 have to be determined by using an iterative process (see below).

Step 3: Assigning coefficients b_2 and b_3 of modified roll and using pinion machine-tool settings obtained in procedure 1, we may determine the pinion tooth surface Σ_1. The gear tooth surface Σ_2 is considered as given.

Step 4: Applying TCA for simulation of meshing of Σ_1 and Σ_2, we may obtain numerically the modified function of transmission errors and then represent it again by polynomial function (1.31) with new magnitudes of coefficients a_0, a_1, a_2, and a_3.

Procedure 2 with steps 1 to 4 has to be repeated until a parabolic function of transmission errors $\Delta\phi_2^{(1)}(\phi_1)$ with limited magnitude of maximal transmission errors is obtained.

The computation is an iterative process based on application of secant method of numerical computations [13]. The goal is to transform the shape of obtained function $\Delta\phi_2^{(1)}(\phi_1)$ of transmission errors into a parabolic function

$$\Delta\phi_2(\phi_1) = -a_2\phi_1^2\,, \qquad -\frac{\pi}{N_1} \le \phi_1 \le \frac{\pi}{N_1} \tag{1.33}$$

where

$$\left|\Delta\phi_2(\phi_1)\right|_{max} = a_2\left(\frac{\pi}{N_1}\right)^2 = \Delta\Phi \tag{1.34}$$

This goal is accomplished by variation of coefficients b_2 and b_3 of function (1.32) provided by modified roll. The variation of b_2 and b_3 is performed independently and is illustrated by drawings of Fig. 1.17.
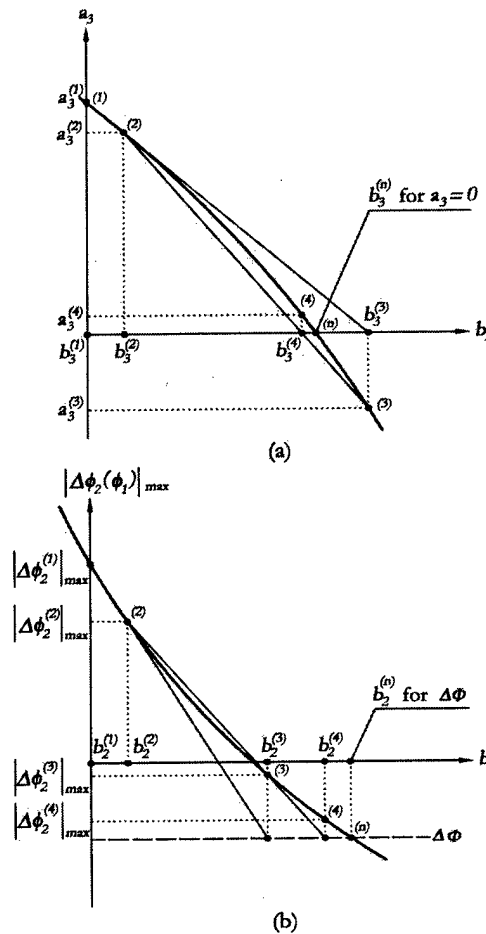

Figure 1.17: Illustration of variation of coefficients b_2 and b_3 of modified roll.

Figure 1.17(a) illustrates variation of coefficient b_3 of modified roll to obtain coefficient $a_3 = 0$ of function (1.31). Function $a_2(b_2)$ is determined as the output of TCA by variation of modified roll.

Figure 1.17(b) illustrates variation of coefficient b_2 of modified roll for obtaining of $\left|\Delta\phi_2(\phi_1)\right|_{max} = \Delta\Phi$.

Function $\Delta\phi_2(\phi_1)$ is determined as the output of TCA by variation of b_2.

Procedure 3. Procedures 1 and 2 are performed by simultaneous application of computational algorithms of local synthesis and TCA, but the errors of alignment are considered at these procedures as equal to zero.

The purpose of procedure 3 is to adjust the gear drive to the existence of errors of alignment. This is achieved by adjusting the previously designed path of contact to the assigned or expected errors of alignment. The procedure is based on the flow chart shown in Fig. 1.18.
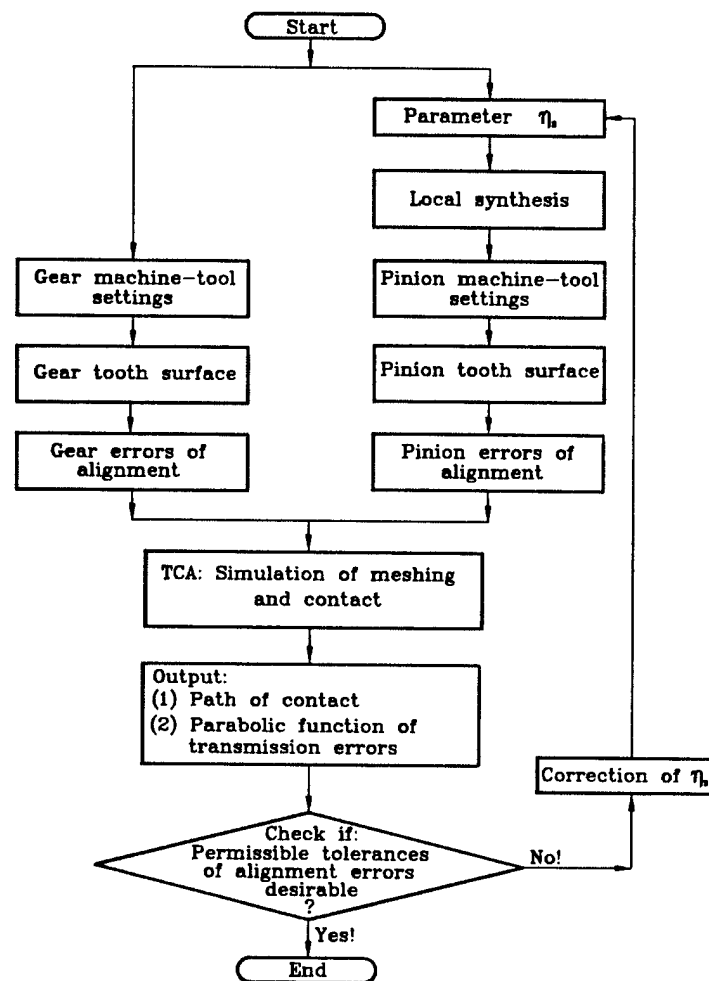

Figure 1.18: Flow chart of procedure 3.

The adjustment of the gear drive to the errors of alignment is performed by correction of parameter η_2 (Fig. 1.12) that determines the orientation of the path of contact on the gear tooth surface.

The prescribed procedure yields that in some cases of design it becomes necessary to deviate the path of contact from the longitudinal direction to reduce the shift of bearing contact caused by errors of alignment. The procedure has to be

applied for separate simulation of each error of alignment for obtaining the required correction of η_2. The permissible tolerance of each alignment error is obtained by procedure 3.

Procedure 4. The purposes of procedure 4 are investigation of formation of bearing contact and determination of contact and bending stresses for more than one cycle of meshing. The goals are obtained by application of the finite element method by the general purpose finite element computer program ABAQUS.

Investigation of formation of bearing contact enables to discover hidden areas of severe contact due to the elastic deformation of the gear teeth. Such a contact may be discovered if finite element models of several pairs of teeth are developed and analyzed in contact positions corresponding to more than one cycle of meshing. Such contact positions are obtained by application of TCA computer program.

Hidden areas of severe contact are accompanied with a substantial increase of contact stresses. Those areas of severe contact might be avoided by increasing the mismatch of generating surfaces. We could obtain such goal by application of combination of straight-line profile blades with parabolic profile blades of the pair of head-cutters that generate the pinion and the gear, respectively.

1.6 Local Synthesis and Determination of Pinion Machine Tool Settings

As a reminder, the local synthesis is accomplished simultaneously with the TCA, and the computation is an iterative process. The computer program developed permits the determination of the pinion machine-tool settings at each iteration.

The input parameters for the local synthesis are the gear machine-tool settings and parameters η_2, a, and m'_{12} (see flow chart, Fig. 1.14).

The procedure of the local synthesis is as follows:

Stage 1: Determination of the mean contact point on the gear tooth surface

Step 1: Mean point A on surface Σ_2 is chosen by designation of parameters L_A and R_A (Fig. 1.19), where A is the candidate for the mean contact point M of surfaces Σ_2 and Σ_1. Then we obtain the following system of two equations in two unknowns

$$Z_2(u_g^*, \theta_g^*) = L_A \tag{1.35}$$

$$X_2^2(u_g^*, \theta_g^*) + Y_2^2(u_g^*, \theta_g^*) = R_A^2$$

where X_2, Y_2, and Z_2 are the projections of position vector $\mathbf{r}_2(u_g^*, \theta_g^*)$.
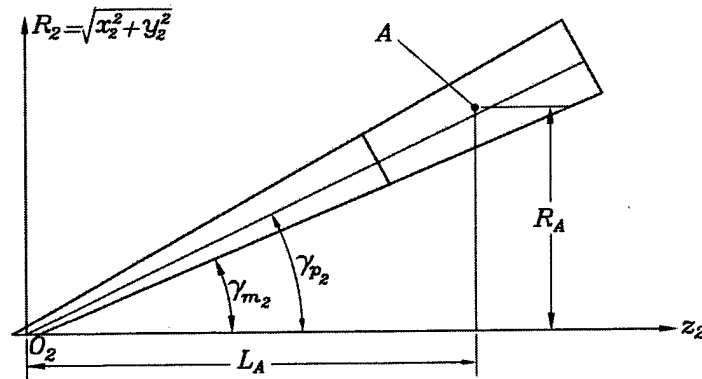

Figure 1.19: Representation of point A in coordinate system S_2.

Step 2: Equations (1.35) considered simultaneously allow us to determine surface parameters (u_g^*, θ_g^*) for point A. Vector functions $\mathbf{r}_g(u_g, \theta_g)$ and $\mathbf{n}_g(\theta_g)$ determine the position vector and surface unit normal for a current point of gear tooth surface Σ_g. Taking in these vector functions $u_g = u_g^*$ and $\theta_g = \theta_g^*$, we can determine the position vector $\mathbf{r}_g^{(A)}$ of point A and the surface unit normal $\mathbf{n}_g^{(A)}$ at A.

Step 3: Parameters u_g^* and θ_g^* and the unit vectors $\mathbf{e}_g$ and $\mathbf{e}_u$ of principal directions on surface Σ_g are considered as known. Here:

$$\mathbf{e}_g = \frac{\partial \mathbf{r}_g^{(A)}}{\partial s_g} \div \left| \frac{\partial \mathbf{r}_g^{(A)}}{\partial s_g} \right| = \begin{bmatrix} -\cos\alpha_g + 2a_c u_g \sin\alpha_g \\ (\pm\sin\alpha_g \pm 2a_c u_g \cos\alpha_g)\sin\theta_g \\ (\pm\sin\alpha_g \pm 2a_c u_g \cos\alpha_g)\cos\theta_g \end{bmatrix} \div \sqrt{1 + 4a_c^2 u_g^2} \tag{1.36}$$

$$\mathbf{e}_u = \frac{\partial \mathbf{r}_g^{(A)}}{\partial \theta_g} \div \left| \frac{\partial \mathbf{r}_g^{(A)}}{\partial \theta_g} \right| = \begin{bmatrix} 0 \\ \cos\theta_g \\ -\sin\theta_g \end{bmatrix} \tag{1.37}$$

The gear generating surface is a surface of revolution, and the principal curvatures k_g and k_u of Σ_g are determined by the following equations:

$$k_g = \frac{2a_c}{(1 + 4a_c^2 u_g^2)^{3/2}}$$

$$k_u = \frac{-\cos\alpha_g + 2a_c u_g \sin\alpha_g}{\left(R_g \pm s_{g0}\sin\alpha_g \pm u_g \sin\alpha_g \pm a_c u_g^2 \cos\alpha_g \right)\sqrt{1 + 4a_c^2 u_g^2}} \tag{1.38}$$

The upper and lower signs correspond to the concave and convex sides of gear tooth, respectively.

The unit vectors $\mathbf{e}_s$ and $\mathbf{e}_q$ of principal directions on surface Σ_2 are obtained by using matrix transformation from S_g to S_2. The gear principal curvatures k_s and k_q of Σ_2 are the same as the principal curvatures k_g and k_u, respectively, of the gear head-cutter.

Stage 2: Tangency of Surfaces $\Sigma_2(\Sigma_g)$ and Σ_1 at Mean Contact Point M.

Step 1: The derivations accomplished at stage 1 permit the position vector $\mathbf{r}_2^{(A)}$ and the surface unit normal $\mathbf{n}_2^{(A)}$ of point A of tangency of surfaces $\Sigma_2(\Sigma_g)$ to be determined. The goal now is to determine such a point M in the fixed coordinate system S_f (Fig. 1.20) where two surfaces $\Sigma_2(\Sigma_g)$ and Σ_1 are in tangency with each other.

Surfaces Σ_2 and Σ_g are the same ones, because there is no relative motion between the cradle and workpiece (between coordinate system S_2 to S_g) whereas the gear is generated. Using coordinate transformation from S_2 to S_f (Fig. 1.20), we may obtain $\mathbf{r}_f^{(A)}$ and $\mathbf{n}_f^{(A)}$. The new position of point A in S_f will become point M of tangency of Σ_2 and Σ_1, if the following equation of meshing between Σ_2 and Σ_1 is observed

$$\mathbf{n}_f^{(A)}\left(\phi_2^{(0)}\right) \cdot \mathbf{v}_f^{(21,A)}\left(\phi_2^{(0)}\right) = 0 \tag{1.39}$$

Here, $\mathbf{n}_f^{(A)} \equiv \mathbf{n}_f^{(M)}$ and $\mathbf{v}_f^{(21,A)} \equiv \mathbf{v}_f^{(21,M)}$; $\mathbf{v}_f^{(21,A)}$ is the relative velocity at point A determined with the ideal gear ratio

$$m_{21}^{(0)} = \frac{\omega^{(2)}}{\omega^{(1)}} \tag{1.40}$$

The solution of equation (1.39) for $\phi_2^{(0)}$ provides the value of the turning angle $\phi_2^{(0)}$. It is evident that two surfaces Σ_2 and Σ_1 are now in tangency with each other at point M.
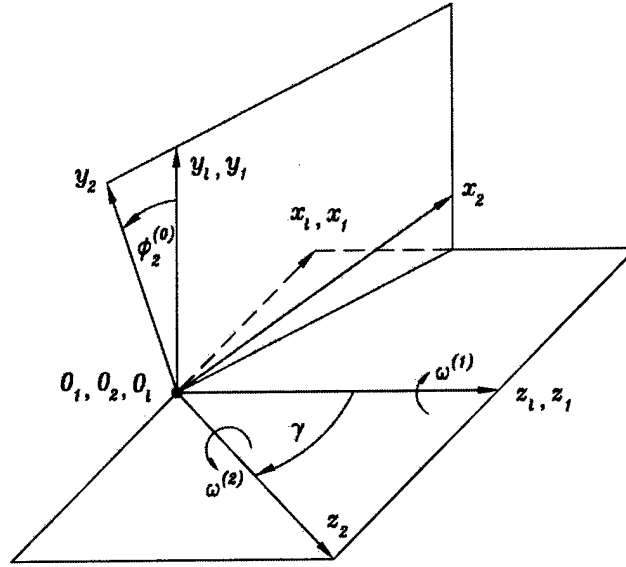
Figure 1.20: Coordinate systems S_2, S_l, and S_1 applied for local synthesis.

Step 2: Consider at point M that the principal curvatures k_s and k_q of surface Σ_2, and the unit vectors e_s and e_q of principal directions on Σ_2 are all know. The unit vectors e_s and e_q are represented in S_l. The goal now is to determine at point M the principal curvatures k_f and k_h of surface Σ_1, and the unit vectors e_f and e_h of principal directions on Σ_1. This goal can be achieved by application of the procedure described in Section 1.7. It is shown in Section 1.7 that the determination of k_f, k_h, e_f and e_h becomes possible if parameters m'_{12}, η_2 (or η_1), and a/δ are assumed to be known or are used as input data.

Stage 3: Tangency of Surfaces $\Sigma_2(\Sigma_g)$, Σ_1, and Σ_p at Mean Contact Point M.

Basic Equations: Tangency of $\Sigma_2(\Sigma_g)$ and Σ_1 at mean contact point M has been already provided at the previous stages. The position vector $r_l^{(M)}$ of point M and the surface unit normal $n_l^{(M)}$ at point M were determined in coordinate system S_l. Let imagine now that coordinate system S_1 (it coincides with S_l) and surface Σ_1 are installed in coordinate system S_{m_1} (Fig. 1.8). Let angle $\psi_1^{(0)}$ (it is the initial value of ψ_1) be the installment angle of the pinion. Using coordinate transformation from S_1 to S_{m_1}, we may determine in S_{m_1} position vector $r_{m_1}^{(M)}$ of point M and the surface unit normal $n_{m_1}^{(M)}$. The conditions of improved meshing and contact of pinion and gear tooth surfaces Σ_1 and Σ_2 are considered in Section 1.7 and then the relationships between the principal curvatures and directions of surfaces for such conditions of meshing and contact are determined (see Eqs. (1.81)). The point of tangency of surfaces Σ_1 and Σ_p is designated in Section 1.7 as point B. The pinion generating surface Σ_p is installed in S_{m_1} taking the cradle angle ψ_{c_1} equal to zero. The position vector of point B of surface Σ_p and the surface unit normal at B are represented in S_{m_1} as $r_{m_1}^{(B)}$ and $n_{m_1}^{(B)}$. The tangency of Σ_1 and Σ_p at the mean contact point M is satisfied, if the following vector equations are observed

$$n_{m_1}^{(M)} = n_{m_1}^{(B)} \qquad (1.41)$$

$$r_{m_1}^{(M)} = r_{m_1}^{(B)} \qquad (1.42)$$

$$n_{m_1}^{(M)} \cdot v_{m_1}^{(1p)} = 0 \qquad (1.43)$$

where equation (1.43) is the equation of meshing. Observation of equations (1.41) to (1.43) means that all of the three surfaces ($\Sigma_2(\Sigma_g)$, Σ_1 and Σ_p) are in contact at point M.

Using equations (1.41) to (1.43) and (1.81), it becomes possible to obtain the settings of the pinion and the head-cutter that guarantee the improved conditions of meshing and contact at point M. The machine tool settings to be determined are as follows:

(i) X_{B_1}, E_{m_1}, X_{D_1} and $m_{1p} = \omega^{(1)}/\omega^{(p)}$. Settings X_{B_1} and X_{D_1} are related by the following equation (Fig. 1..21)

$$X_{B_1} = -\left(X_{D_1} - \left|\overline{O_R O_1}\right|\right)\sin\gamma_{m_1} \tag{1.44}$$

where

$$\left|\overline{O_R O_1}\right| = \frac{\left[(A_m + F_w/2)\sin\gamma_1 - a_{d_1}\cos\gamma_1\right]}{\tan\gamma_{m_1}} - \left[(A_m + F_w/2)\cos\gamma_1 + a_{d_1}\sin\gamma_1\right]$$

Equation (1.44) is determined for the case of design of a spiral bevel gear with different apexes of the pitch and root cones.
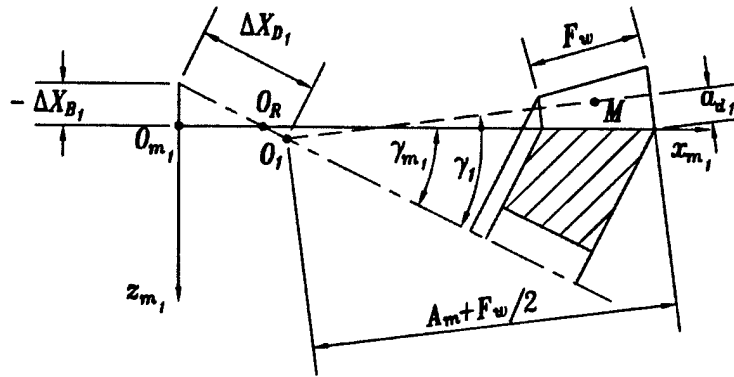

Figure 1.21: For derivation of pinion machine tool settings.

(ii) Design parameter R_p of the head-cutter (Fig. 1.10).

(iii) Parameters S_{r_1} and q_1 that determine the installment of the head-cutter on the cradle (Fig. 1.9).

(iv) Parameter $\psi_1^{(0)}$ that is the initial angle ψ_1 for installment of coordinate system S_1 with respect to S_{b_1} (Fig. 1.8), and parameter θ_p of the head-cutter surface Σ_p.

Computation of Pinion Machine-Tool Settings. The procedure for computation is as follows:

Step 1: Determine the values of θ_p and $\psi_1^{(0)}$ that are the sought-for two unknowns in Equations (1.41)-(1.43). Equation (1.41) is used for determination of θ_p and $\psi_1^{(0)}$, taking into account that

$$\mathbf{n}_{m_1}^{(M)}(\theta_p) = \begin{bmatrix} \cos\alpha_p\cos\theta_p \\ \cos\alpha_p\sin\theta_p \\ \mp\sin\alpha_p \end{bmatrix} \tag{1.45}$$

and

$$\mathbf{n}_{m_1}^{(M)} = \mathbf{L}_{m_1 b_1}\mathbf{L}_{b_1 1}\mathbf{n}_1^{(M)} \tag{1.46}$$

where $\mathbf{n}_1^{(M)} \equiv \mathbf{n}_l^{(M)}$ since S_1 coincides with S_l (Fig. 1.20). Here,

$$\mathbf{L}_{m_1 b_1} = \begin{bmatrix} \sin\gamma_{m_1} & 0 & \cos\gamma_{m_1} \\ 0 & 1 & 0 \\ -\cos\gamma_{m_1} & 0 & \sin\gamma_{m_1} \end{bmatrix} \tag{1.47}$$

$$\mathbf{L}_{b_1 1} = \begin{bmatrix} \cos\psi_1^{(0)} & -\sin\psi_1^{(0)} & 0 \\ \sin\psi_1^{(0)} & \cos\psi_1^{(0)} & 0 \\ 0 & 0 & 1 \end{bmatrix} \tag{1.48}$$

Equations (1.41) and (1.45)-(1.48) yield the following expressions for determination of θ_p and $\psi_1^{(0)}$

$$\cos\theta_p = \frac{n_{lz} \pm \sin\gamma_{m_1}\sin\alpha_p}{\cos\gamma_{m_1}\cos\alpha_p} \tag{1.49}$$

$$\sin\psi_1^{(0)} = \frac{-n_{ly}\cos\theta_p\cos\alpha_p + n_{lx}\sin\gamma_{m_1}\sin\theta_p\cos\alpha_p + n_{ly}n_{lz}\cos\gamma_{m_1}}{\sin\gamma_{m_1}\left(n_{lx}^2 + n_{ly}^2\right)} \tag{1.50}$$

$$\cos\psi_1^{(0)} = \frac{\sin\theta_p\cos\alpha_p - n_{lx}\sin\psi_1^{(0)}}{n_{ly}} \tag{1.51}$$

where α_p is the given value of the profile angle of the head-cutter, and n_{lx}, n_{ly}, and n_{lz} are the three components of vector $\mathbf{n}_l^{(M)}$. The great advantage of the approach developed and discussed above is that the requirement of the coincidence of the normals does not require a non-standard profile angle α_p or the tilt of the head-cutter with respect to the cradle.

Using θ_p, it becomes possible to determine the unit vectors $\mathbf{e}_p$ and $\mathbf{e}_t$ of principal directions on surface Σ_p at point M.

Step 2: Determination of pinion machine-tool settings $X_{B_1}(X_{D_1})$, E_{m_1}, m_{1p} and the design parameter R_p of the head-cutter (five unknowns are sought-for).

As a reminder, X_{B_1} and X_{D_1} are related by equation (1.44). The determination of the machine-tool settings mentioned above is based on application of the system of equations (1.81) and equation (1.43) that represent a system of four non-linear equations with four unknowns: X_{D_1}, E_{m_1}, m_{1p} and R_p.

The design parameters mentioned above provide as well improved conditions of meshing and contact at the mean contact point M.

Step 3: Determination of machine-tool settings S_{r_1} and q_1 and the pinion surface parameter s_p (three unknowns are sought-for).

Determination of the mentioned three parameters is based on application of equation (1.42), considering that generating surface Σ_p is a cone. The final equations for the pinion are as follows:

$$S_{r_1}\cos q_1 + \left(R_p \mp s_p\sin\alpha_p\right)\cos\theta_p = X_{m_1}^{(M)} \tag{1.52}$$

$$S_{r_1}\sin(\pm q_1) + \left(R_p \mp s_p\sin\alpha_p\right)\sin\theta_p = Y_{m_1}^{(M)} \tag{1.53}$$

$$-s_p\cos\alpha_p = Z_{m_1}^{(M)} \tag{1.54}$$

The upper and lower signs in equation (1.53) correspond to the design of right-hand and left-hand pinions, respectively.

The stages of computation discussed above may be summarized as follows:

(i)   It is necessary to determine ten unknowns: six machine-tool settings ($X_{B_1}, E_{m_1}, X_{D_1}, q_1, S_r, m_{1p}$), two surface parameters $\left(\theta_p, s_p\right)$, one cutter parameter R_p and one position parameter $\psi_1^{(0)}$ which defines the pinion initial turn angle.

(ii)   The equation system for determination of the unknowns is formed as follows:

$$\mathbf{n}_{m_1}^{(M)} = \mathbf{n}_{m_1}^{(B)} \qquad (1.55)$$

$$\mathbf{r}_{m_1}^{(M)} = \mathbf{r}_{m_1}^{(B)} \qquad (1.56)$$

$$\mathbf{n}_{m_1}^{(M)} \cdot \mathbf{v}_{m_1}^{(1p)} = 0 \qquad (1.57)$$

$$X_{B_1} = -\left(X_{D_1} - \left|\overline{O_r O_1}\right|\right)\sin\gamma_{m_1} \qquad (1.58)$$

In addition, we use three curvature equations

$$\tan 2\sigma^{(1p)} = \frac{-2d_{13}d_{23}}{d_{23}^2 - d_{13}^2 - (k_f - k_h)d_{33}}$$

$$k_t - k_p = \frac{-2d_{13}d_{23}}{d_{33}\sin 2\sigma^{(1p)}} \qquad (1.59)$$

$$k_t + k_p = k_f + k_h + \frac{d_{13}^2 + d_{23}^2}{d_{33}}$$

Equation (1.55) is equivalent to two independent scalar equations, equations (1.56) are equivalent to three scalar equations, equations (1.57), (1.58), and (1.59) represent five scalar equations. Thus, the system of equations provides indeed ten scalar equations for determination of ten unknowns. The solution for the unknowns requires: (i) solution of a subsystem of four nonlinear equations (see step 2), and (ii) solution of six remaining equations represented in echelon form (each of the six equations contains one unknown to be determined).

1.7 Relationships Between Principal Curvatures and Directions of Mating Surfaces

The procedure of local synthesis requires the knowledge of principal curvatures and directions of contacting surfaces. In the case of design discussed above, the pinion tooth surface is represented by three related parameters and the determination of pinion principal curvatures and directions is a complex problem. The solution to the problem is simplified by presentation of pinion principal curvatures and directions in terms of principal curvatures and directions of the head-cutter and parameters of motions of the generating process (proposed in [2, 7]).

Important relations between principal curvatures and directions of mating surfaces being in point contact (proposed in [2, 7]) are applied for local synthesis (see Section 1.6).

Henceforth two types of instantaneous contact of meshing surfaces will be considered: (i) along a line, and (ii) at a point. Line contact is provided in meshing of the surface being generated with the tool surface. Point contact is provided for meshing of the generated pinion and gear tooth surfaces. The determination of the required relationships is based on the approach proposed in [4, 7]. The basic equations in the approach developed are as follows (see the nomenclature):

$$\mathbf{v}_r^{(2)} = \mathbf{v}_r^{(1)} + \mathbf{v}^{(12)} \qquad (1.60)$$

$$\dot{\mathbf{n}}_r^{(2)} = \dot{\mathbf{n}}_r^{(1)} + \boldsymbol{\omega}^{(12)} \times \mathbf{n} \qquad (1.61)$$

$$\frac{d}{dt}\left[\mathbf{n} \cdot \mathbf{v}^{(12)}\right] = 0 \qquad (1.62)$$

Equations (1.60) and (1.61) relate the velocities of the contact point and the tip of the unit normal in their motions over the contacting surfaces. Equation (1.62) represents the differentiated equation of meshing. Equations (1.60) to (1.62) yield a skew-symmetric system of three linear equations in two unknowns x_1 and x_2 of the following structure

$$a_{i_1}x_1 + a_{i_2}x_2 = a_{i_3} \qquad (i = 1-3) \qquad (1.63)$$

Here x_1 and x_2 are the projections of the velocity of the contact point in the motion over one of the surface along the principal directions of the mating surface. In case of line contact of surfaces, the solution for the unknowns is indefinite and the rank of the system matrix of the linear equations is one. In case of point contact of surfaces, the solution for the unknowns is definite, and the rank of the system matrix is two. The properties mentioned above are used for the derivation of the sought for relationships between the principal curvatures and directions of the meshing surfaces.

Meshing of Surfaces Σ_2 and Σ_1. Surfaces Σ_1 and Σ_2 are in point contact and their meshing is considered in fixed coordinate system S_f (Fig. 1.20). Equations (1.60) to (1.62) yield the following system of three linear equations [4, 7]

$$a_{i_1} v_s^{(1)} + a_{i_2} v_q^{(1)} = a_{i_3} \qquad (i = 1-3) \tag{1.64}$$

where

$$v_s^{(1)} = \mathbf{v}_r^{(1)} \cdot \mathbf{e}_s \qquad v_q^{(1)} = \mathbf{v}_r^{(1)} \cdot \mathbf{e}_q \tag{1.65}$$

$$a_{11} = k_s - k_f \cos^2 \sigma^{(12)} - k_h \sin^2 \sigma^{(12)}$$

$$a_{12} = a_{21} = 0.5\left(k_f - k_h\right)\sin 2\sigma^{(12)}$$

$$a_{13} = a_{31} = -k_s v_s^{(12)} + \left[\left(\mathbf{n} \times \boldsymbol{\omega}^{(12)}\right) \cdot \mathbf{e}_s\right]$$

$$a_{22} = k_q - k_f \sin^2 \sigma^{(12)} - k_h \cos^2 \sigma^{(12)} \tag{1.66}$$

$$a_{23} = a_{32} = -k_q v_q^{(12)} + \left[\left(\mathbf{n} \times \boldsymbol{\omega}^{(12)}\right) \cdot \mathbf{e}_q\right]$$

$$a_{33} = k_s \left(v_s^{(12)}\right)^2 + k_q \left(v_q^{(12)}\right)^2 - \left[\left(\mathbf{n} \times \boldsymbol{\omega}^{(12)}\right) \cdot \mathbf{v}^{(12)}\right]$$
$$\quad - \mathbf{n} \cdot \left[\left(\boldsymbol{\omega}^{(1)} \times \mathbf{v}_{tr}^{(2)}\right) - \left(\boldsymbol{\omega}^{(2)} \times \mathbf{v}_{tr}^{(1)}\right)\right] + m'_{12}\left(\mathbf{n} \times \mathbf{k}_2\right) \cdot \mathbf{r}$$

It is considered as known in the following considerations: point M of tangency of surfaces Σ_1 and Σ_2, the common surface unit normal, the relative velocity $\mathbf{v}^{(12)}$, the principal curvatures k_s and k_q and directions $\mathbf{e}_s$ and $\mathbf{e}_q$ on Σ_2 at M, and the elastic deformation δ of surfaces at M. The goal is to determine the principal curvatures k_f and k_h and the angle $\sigma^{(12)}$ formed by the unit vectors $\mathbf{e}_f$ and $\mathbf{e}_s$.

The velocity $\mathbf{v}_r^{(i)}$ $(i = 1,2)$ of the contact point in motion over surface Σ_i has a definite direction and therefore the rank of the system matrix (1.64) is one. This property yields the following relation:

$$\begin{vmatrix} a_{11} & a_{12} & a_{13} \\ a_{21} & a_{22} & a_{23} \\ a_{31} & a_{32} & a_{33} \end{vmatrix} = F(k_f, k_h, k_s, k_q, \sigma^{(12)}, m'_{12}) = 0 \tag{1.67}$$

The sought-for solution for k_f, k_h, and $\sigma^{(12)}$ can be obtained if the following parameters will be chosen: the derivative m'_{12}; the ratio a/δ, where a is the major axis of the contact ellipse; the direction at M of the tangent to the contact path on one of the couple of contacting surfaces Σ_1 and Σ_2. The relation between the directions at M of the tangents to the contact paths on both surfaces is represented by the equation [4, 7]

$$\tan \eta_1 = \frac{-a_{13} v_q^{(12)} + \left(a_{33} + a_{13} v_s^{(12)}\right)\tan \eta_2}{a_{33} + a_{23}\left(v_q^{(12)} - v_s^{(12)} \tan \eta_2\right)} \tag{1.68}$$

Choosing η_2 at point M, we can determine η_1.

Procedure of Determination of k_f, k_h and $\sigma^{(12)}$

Step 1: Determine η_1 choosing η_2.

Step 2:

$$v_s^{(1)} = \frac{a_{33}}{a_{13} + a_{23} \tan \eta_1}$$ (1.69)

$$v_q^{(1)} = \frac{a_{33} \tan \eta_1}{a_{13} + a_{23} \tan \eta_1}$$ (1.70)

Step 3:

$$A = \frac{\delta}{a^2}$$ (1.71)

Step 4:

$$K_\Sigma = \frac{\dfrac{a_{13}^2 + a_{23}^2}{\left(v_s^{(1)}\right)^2 + \left(v_q^{(1)}\right)^2} - 4A^2}{\dfrac{a_{13}v_s^{(1)} + a_{23}v_q^{(1)}}{\left(v_s^{(1)}\right)^2 + \left(v_q^{(1)}\right)^2} + 2A}$$ (1.72)

Step 5:

$$\begin{bmatrix} a_{11} \\ a_{12} \\ a_{22} \end{bmatrix} = \frac{1}{\left(v_s^{(1)}\right)^2 + \left(v_q^{(1)}\right)^2} \begin{bmatrix} a_{13}v_s^{(1)} - a_{23}v_q^{(1)} + \left(v_q^{(1)}\right)^2 K_\Sigma \\ a_{13}v_q^{(1)} + a_{23}v_s^{(1)} - v_s^{(1)}v_q^{(1)} K_\Sigma \\ -a_{13}v_s^{(1)} + a_{23}v_q^{(1)} + \left(v_s^{(1)}\right)^2 K_\Sigma \end{bmatrix}$$ (1.73)

Step 6:

$$\tan 2\sigma^{(12)} = \frac{2a_{12}}{g_2 - (a_{11} - a_{22})}$$ (1.74)

where $g_2 = k_s - k_q$.

Step 7:

$$g_1 = \frac{2a_{12}}{\sin 2\sigma^{(12)}}$$ (1.75)

Step 8:

$$K_\Sigma^{(1)} = K_\Sigma^{(2)} - K_\Sigma$$ (1.76)

where $K_\Sigma^{(2)} = k_s + k_q$.

Step 9:

$$k_f = \left(K_\Sigma^{(1)} + g_1\right)/2$$ (1.77)

Step 10:

$$k_h = \left(K_\Sigma^{(1)} - g_1\right)/2$$ (1.78)

The procedure represented above can be used to obtain the sought for principal curvatures k_f and k_h at point M of tangency of surfaces Σ_2 and Σ_1 and the principal directions on Σ_1 at M.

Meshing of Surfaces Σ_1 and Σ_p: The tool surface Σ_p generates the pinion tooth surface Σ_1. Surfaces Σ_p and Σ_1 are in line contact and point B is the chosen point of the instantaneous line of contact. The meshing of surfaces is considered in S_{m_1}. At point B, the following parameters are assumed as known: the curvatures k_f and k_h of surface Σ_1; the unit vectors $\mathbf{e}_f$ and $\mathbf{e}_h$ of principal directions on Σ_1; the surfaces unit normals; the relative velocity $\mathbf{v}^{(12)}$. The goal is to determine the principal curvatures k_p and k_t of surface Σ_p, and the angle $\sigma^{(1p)}$ that is formed by the unit vectors $\mathbf{e}_f$ and $\mathbf{e}_p$.

Equation (1.60) to (1.62) yield a system of three linear equations

$$d_{i_1} v_f^{(p)} + d_{i_2} v_h^{(p)} = d_{i_3} \quad (i = 1 - 3)$$ (1.79)

where

$$v_f^{(p)} = \mathbf{v}_r^{(p)} \cdot \mathbf{e}_f, \qquad v_h^{(p)} = \mathbf{v}_r^{(p)} \cdot \mathbf{e}_h \tag{1.80}$$

The direction of $\mathbf{v}_r^{(p)}$ is indefinite since surfaces Σ_p and Σ_1 are in line contact. Therefore, the rank of system matrix of equations is equal to one. Using this property, the following equations are obtained:

$$\tan 2\sigma^{(1p)} = \frac{-2d_{13}d_{23}}{d_{23}^2 - d_{13}^2 - (k_f - k_h)d_{33}}$$

$$k_t - k_p = \frac{-2d_{13}d_{23}}{d_{33}\sin 2\sigma^{(1p)}} \tag{1.81}$$

$$k_t + k_p = k_f + k_h + \frac{d_{13}^2 + d_{23}^2}{d_{33}}$$

Here

$$d_{13} = -k_f v_f^{(1p)} + \left[\left(\mathbf{n} \times \boldsymbol{\omega}^{(1p)}\right) \cdot \mathbf{e}_f\right]$$

$$d_{23} = -k_h v_h^{(1p)} + \left[\left(\mathbf{n} \times \boldsymbol{\omega}^{(1p)}\right) \cdot \mathbf{e}_h\right]$$

$$d_{33} = -k_f \left(v_f^{(1p)}\right)^2 - k_h \left(v_h^{(1p)}\right)^2 + \left[\left(\mathbf{n} \times \boldsymbol{\omega}^{(1p)}\right) \cdot \mathbf{v}^{(1p)}\right] \tag{1.82}$$

$$\qquad - \mathbf{n} \cdot \left[\left(\boldsymbol{\omega}^{(1)} \times \mathbf{v}_{tr}^{(p)}\right) - \left(\boldsymbol{\omega}^{(p)} \times \mathbf{v}_{tr}^{(1)}\right)\right]$$

where

$$v_f^{(1p)} = \mathbf{v}^{(1p)} \cdot \mathbf{e}_f, \qquad v_h^{(1p)} = \mathbf{v}^{(1p)} \cdot \mathbf{e}_h \tag{1.83}$$

1.8 Simulation of Meshing and Contact Accomplished in Procedure 1 (Section 1.5)

The main goal of simulation of meshing and contact in procedure 1 (see flow chart of Fig. 1.14) is the determination of bearing contact that corresponds to pinion machine-tool settings obtained in Section 1.6. Recall that the computational procedures represented in Sections 1.5 and 1.6 must be applied simultaneously, to represent an iterative process for determination of longitudinal path of contact. The developed TCA (Tooth Contact Analysis) computer program (based on simulation of meshing and contact) allows us to obtain at each stage of iteration the path of contact. In addition, TCA enables us to obtain the function of transmission errors which shape has to be corrected by application of pinion modified roll (see procedure 2 of Section 1.5).

Applied Coordinate Systems. The meshing of gear tooth surfaces is considered in the fixed coordinate system S_h that is rigidly connected to the housing (Fig. 1.22). Movable coordinate system S_1 and S_2 are rigidly connected to the pinion and the gear, respectively. Auxiliary coordinate systems S_{b_1} and S_{b_2} are used for representation of the rotation of the pinion (with respect to S_{b_1}) and the gear (with respect to S_{b_2}). The errors of alignment are simulated by respective installment of S_{b_1} and S_{b_2} with respect to S_h.

The errors of installment are: ΔA_1 –the axial displacement of the pinion; $\Delta\gamma$ –the change of the shaft angle γ; ΔE –the shortest distance between the axes of the pinion and the gear when the pinion-gear axes are crossed instead of intersected; ΔA_2 –the axial displacement of the gear. In the case of an aligned gear drive, we consider that ΔA_1, $\Delta\gamma$, ΔE, and ΔA_2 are all equal to zero.

Simulation Algorithm. During the process of meshing, the pinion and gear tooth surfaces must be in continuous tangency and this condition can be provided if at any instant their position vectors coincide and the surface normals are collinear. Instead of collinearity of surface normals, equality of surface unit normals may be required.
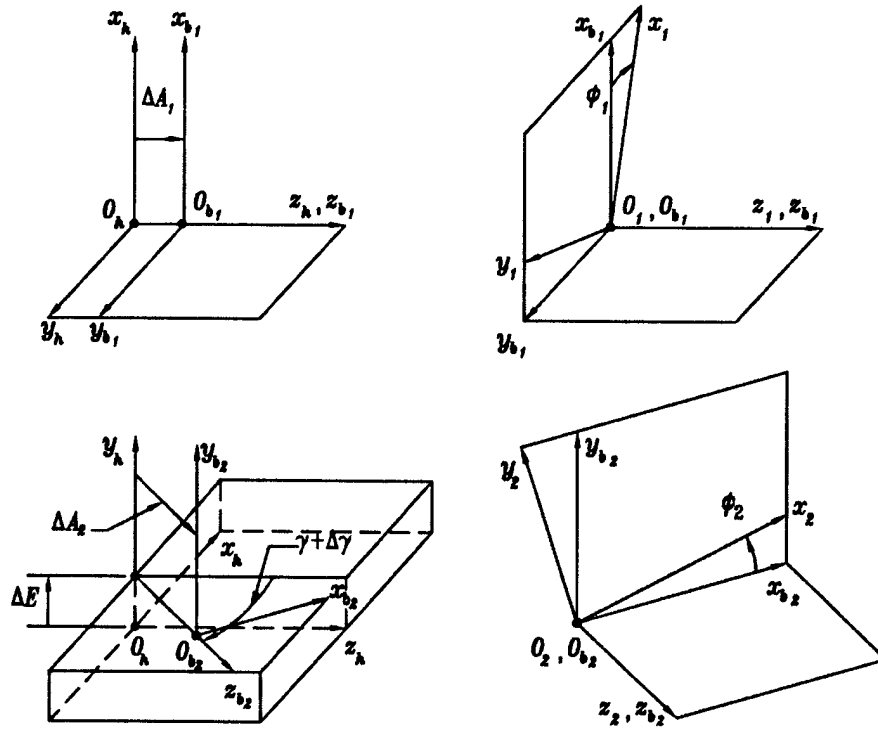
Figure 1.22: Coordinate systems applied for simulation of meshing of pinion and gear tooth surfaces.

Pinion and gear tooth surfaces are represented in coordinate system S_h by the following equations

$$\mathbf{r}_h^{(1)}(s_p,\theta_p,\psi_1,\phi_1) = \mathbf{M}_{hb_1}\mathbf{M}_{b_1 1}(\phi_1)\mathbf{r}_1(s_p,\theta_p,\psi_1) \tag{1.84}$$

$$\mathbf{r}_h^{(2)}(u_g,\theta_g,\phi_2) = \mathbf{M}_{hb_2}\mathbf{M}_{b_2 2}(\phi_2)\mathbf{r}_2(u_g,\theta_g) \tag{1.85}$$

Here

$$\mathbf{M}_{b_1 1} = \begin{bmatrix} \cos\phi_1 & \sin\phi_1 & 0 & 0 \\ -\sin\phi_1 & \cos\phi_1 & 0 & 0 \\ 0 & 0 & 1 & 0 \\ 0 & 0 & 0 & 1 \end{bmatrix}$$

$$\mathbf{M}_{hb_1} = \begin{bmatrix} 1 & 0 & 0 & 0 \\ 0 & 1 & 0 & 0 \\ 0 & 0 & 1 & \Delta A_1 \\ 0 & 0 & 0 & 1 \end{bmatrix}$$

$$\mathbf{M}_{b_2 2} = \begin{bmatrix} \cos\phi_2 & -\sin\phi_2 & 0 & 0 \\ \sin\phi_2 & \cos\phi_2 & 0 & 0 \\ 0 & 0 & 1 & 0 \\ 0 & 0 & 0 & 1 \end{bmatrix}$$

$$\mathbf{M}_{hb_2} = \begin{bmatrix} \cos(\gamma+\Delta\gamma) & 0 & -\sin(\gamma+\Delta\gamma) & -\Delta A_2\sin(\gamma+\Delta\gamma) \\ 0 & 1 & 0 & \Delta E \\ \sin(\gamma+\Delta\gamma) & 0 & \cos(\gamma+\Delta\gamma) & \Delta A_2\cos(\gamma+\Delta\gamma) \\ 0 & 0 & 0 & 1 \end{bmatrix}$$

Unit normals to surfaces of pinion and gear are represented in S_h by the following equations, respectively

$$\mathbf{n}_h^{(1)}(s_p,\theta_p,\psi_1,\phi_1) = \mathbf{L}_{h1}(\phi_1)\mathbf{n}_1(s_p,\theta_p,\psi_1) \tag{1.86}$$

$$\mathbf{n}_h^{(2)}(u_g,\theta_g,\phi_2) = \mathbf{L}_{hb_2}\mathbf{L}_{b_2 2}(\phi_2)\mathbf{n}_2(u_g,\theta_g) \tag{1.87}$$

Here:

$$\mathbf{L}_{h1} = \begin{bmatrix} \cos\phi_1 & \sin\phi_1 & 0 \\ -\sin\phi_1 & \cos\phi_1 & 0 \\ 0 & 0 & 1 \end{bmatrix}$$

$$\mathbf{L}_{b_2 2} = \begin{bmatrix} \cos\phi_2 & -\sin\phi_2 & 0 \\ \sin\phi_2 & \cos\phi_2 & 0 \\ 0 & 0 & 1 \end{bmatrix}$$

$$\mathbf{L}_{hb_2} = \begin{bmatrix} \cos(\gamma+\Delta\gamma) & 0 & -\sin(\gamma+\Delta\gamma) \\ 0 & 1 & 0 \\ \sin(\gamma+\Delta\gamma) & 0 & \cos(\gamma+\Delta\gamma) \end{bmatrix}$$

Conditions of continuous tangency of pinion and gear tooth surfaces are represented by the following equations

$$\mathbf{r}_h^{(1)}(s_p,\theta_p,\psi_1,\phi_1) - \mathbf{r}_h^{(2)}(u_g,\theta_g,\phi_2) = \mathbf{0} \tag{1.88}$$

$$\mathbf{n}_h^{(1)}(s_p,\theta_p,\psi_1,\phi_1) - \mathbf{n}_h^{(2)}(u_g,\theta_g,\phi_2) = \mathbf{0} \tag{1.89}$$

$$f_{1p}^{(a)}(s_p,\theta_p,\psi_1) = 0 \tag{1.90}$$

Surfaces Σ_1 and Σ_2 are represented in S_h by four and three related parameters, respectively. Equation (1.90) is the equation of meshing of the pinion and generating head-cutter and relates the surface parameters of the head-cutter with the generalized parameter ψ_1 of motion of the process of generation of the pinion. Vector equations (1.88), (1.89), and (1.90) yield three, two independent and one scalar equations, respectively. The whole system of equations (1.88) to (1.90) provides six equations for determination of seven unknowns represented as

$$f_i(s_p,\theta_p,\psi_1,\phi_1,u_g,\theta_g,\phi_2) = 0, \qquad f_i \in C^1, \quad (i=1,\cdots,6) \tag{1.91}$$

One of the unknowns, say ϕ_1, is considered as the input parameter in the range

$$\left(-\frac{\pi}{N_1}\right) \le \phi_1 \le \left(\frac{\pi}{N_1}\right)$$

It is assumed that the Jacobian of the system (1.88) to (1.90) differs from zero at each iteration.

The paths of contact on the pinion and the gear tooth surfaces are represented by the following functions:

$$\mathbf{r}_1 = \mathbf{r}_1(s_p(\phi_1),\theta_p(\phi_1),\psi_1(\phi_1)) \tag{1.92}$$

$$f_{1p}^{(a)}(s_p(\phi_1),\theta_p(\phi_1),\psi_1(\phi_1)) = 0 \tag{1.93}$$

and

$$\mathbf{r}_2 = \mathbf{r}_2(u_g(\phi_1),\theta_g(\phi_1)) \tag{1.94}$$

respectively.

The function of transmission errors is defined as

$$\Delta\phi_2(\phi_1) = \phi_2(\phi_1) - \frac{N_1}{N_2}\phi_1 \tag{1.95}$$

The bearing contact is formed as a set of instantaneous contact ellipses. The lengths of the major and minor axes of contact ellipse and their orientation are determined using the approach proposed in [7].

Using vector function (1.94) , we may determine projection L_T of the path of contact on the gear tooth surface in the tangent plane at the mean contact point M . The goal is to obtain L_T as a straight line directed longitudinally. The process of computation is an iterative process and requires simultaneous application of local synthesis and TCA. The errors of alignment in this procedure are not taken into account. The influence of errors of alignment on transmission errors requires additional application of TCA.

It may be discovered in some cases of design, that the gear drive is too sensitive to errors of alignment. Then, it becomes necessary to deviate L_T from the longitudinal directed straight line by correction of η_2 in procedure 3 (see flow chart of Fig. 1.18).

Chapter 2

TCA and FEA Results

2.1 Introduction

In this chapter, the results obtained from computations of tooth contact analysis (TCA) and finite element analysis (FEA) are represented. Several cases of the design of formate-cut spiral bevel gears and face-milled generated spiral bevel gears have been considered for their comparison. A predesigned function of transmission errors of maximum level of 8 arcsec has been considered for all cases of design.

2.2 Design Cases

A face-milled generated spiral bevel gear drive of 19 x 62 teeth has been considered as the baseline design. Our goal is to find an optimized design of this gear drive using the formate cut method providing a predesigned function of transmission errors of low level and a stabilized and longitudinal path of contact. Using the formate-cut method, the productivity of manufacturing of the gear will be increased substantially.

The following cases of design have been considered:

Design GTD1: This case of design is the baseline design with a path of contact directed longitudinally. Gear and pinion are generated by head-cutters with straight profiles.

Design GTD2: In this case of design, the gear is generated with a head-cutter of parabolic profiles whereas the pinion is generated by head-cutters with straight profiles.

Design GTD3: In this case of design, the gear is generated with a head-cutter of straight profiles whereas the pinion is generated by head-cutters with parabolic profiles.

Design FTD1: In this case of design, the formate-cut method is considered for the gear. The head-cutter for the gear has parabolic profiles. The pinion is generated by head-cutters with straight profiles.

Design FTD2: In this case of design, the formate-cut method is considered for the gear as well. The head-cutter that cut the gear has parabolic profiles, but the parabola coefficient is larger. The pinion is generated by head-cutters with straight profiles.

2.3 Results of Tooth Contact Analysis (TCA)

Only results of tooth contact analysis for the convex side of the gear in mesh with the concave side of the pinion will be shown. Similar results can be obtained for the concave side of the gear in mesh with the convex side of the pinion.

Figure 2.1 shows the path of contact and the function of transmission errors for the baseline design. Figures 2.2 and 2.3 show the path of contact and the function of transmission errors for designs GTD2 and GTD3, respectively. Figures 2.4 and 2.5 show the path of contact and the function of transmission errors for designs FTD1 and FTD2, respectively, based on the formate cut method.
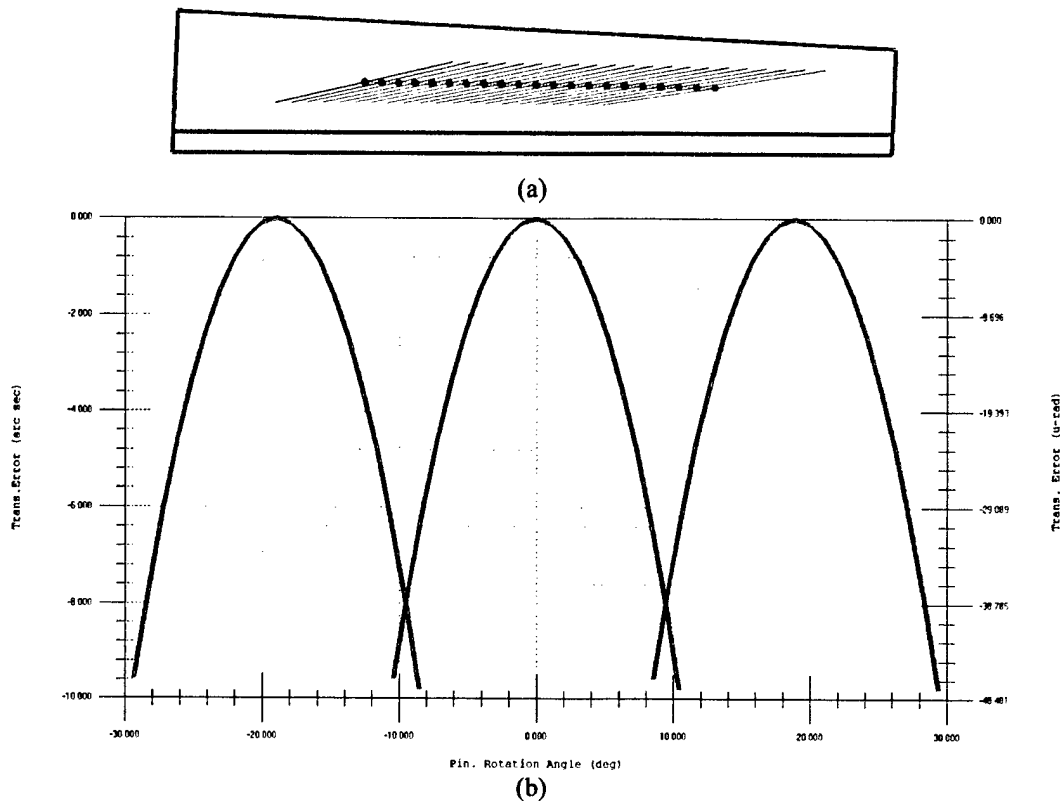
Figure 2.1. (a) Path of contact and (b) function of transmission errors for case of design GTD1, considered as well as the baseline design.
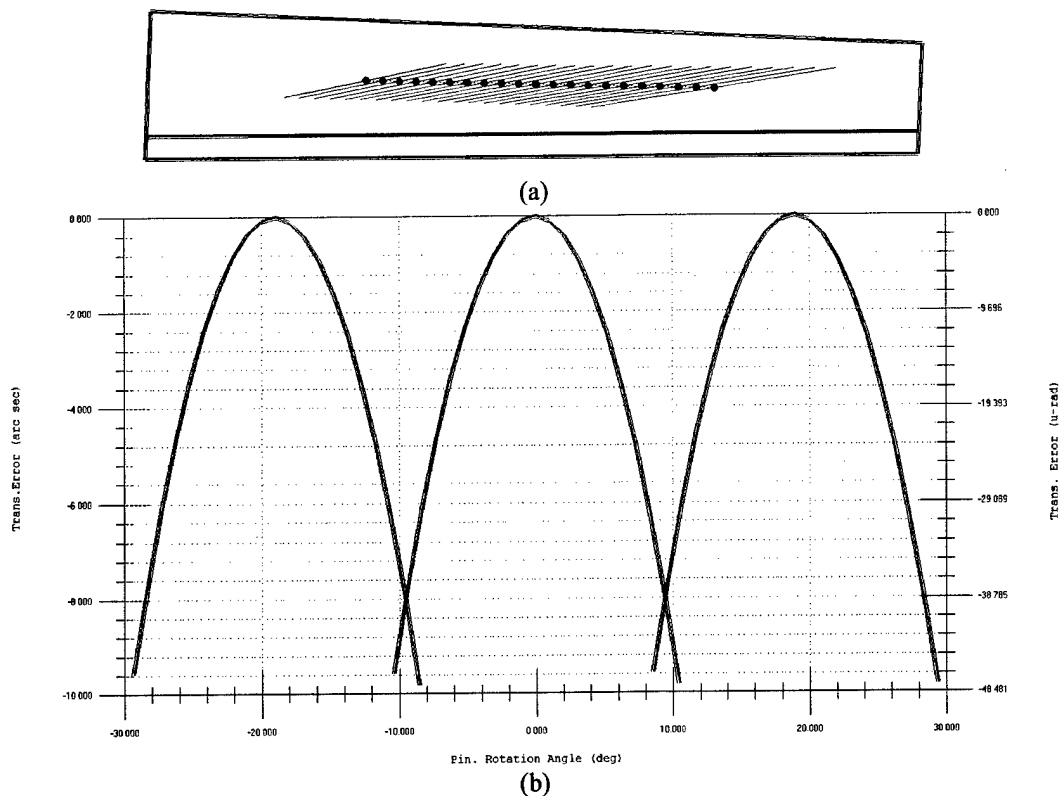
Figure 2.2. (a) Path of contact and (b) function of transmission errors for case of design GTD2.
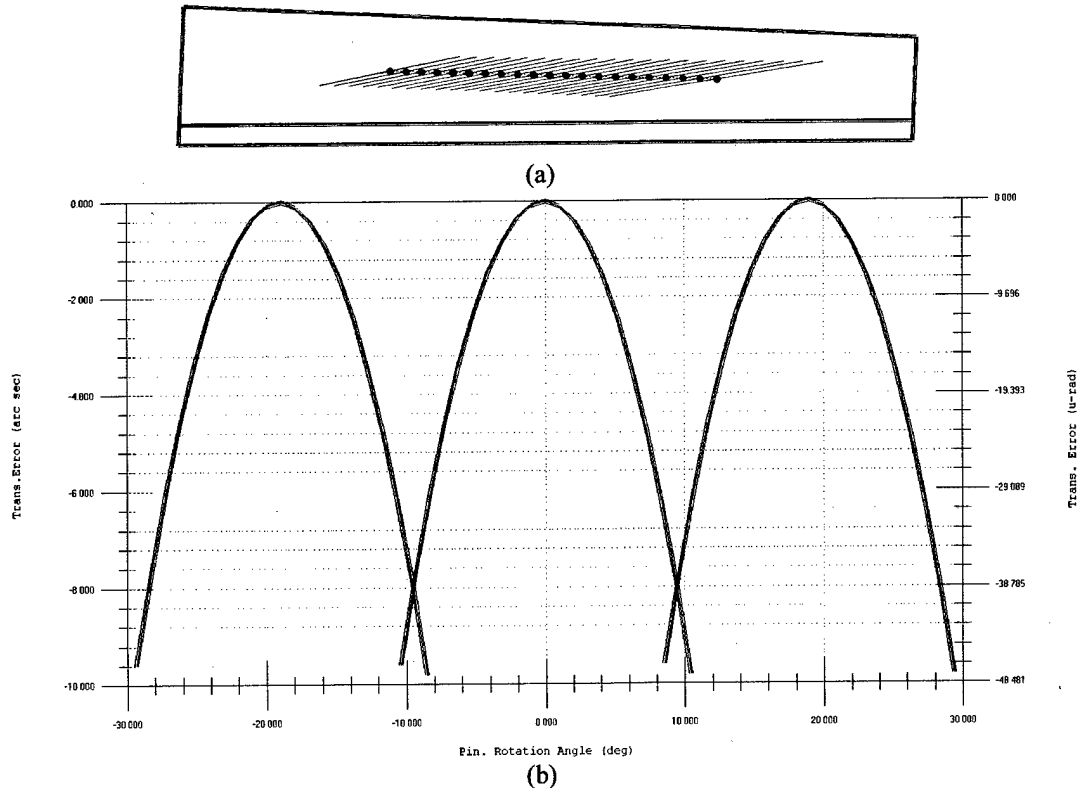
Figure 2.3.(a) Path of contact and (b) function of transmission errors for GTD3 design.

(a)

(b)
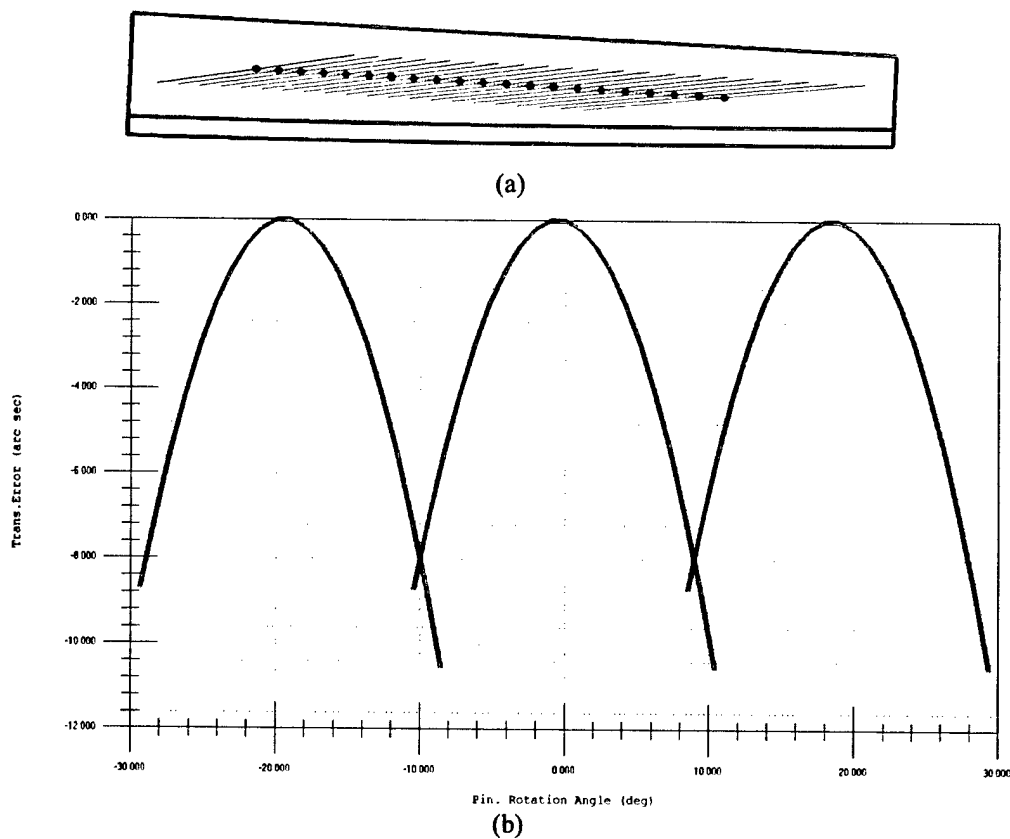
Figure 2.4. (a) Path of contact and (b) function of transmission errors for FTD1 design.

(a)

(b)
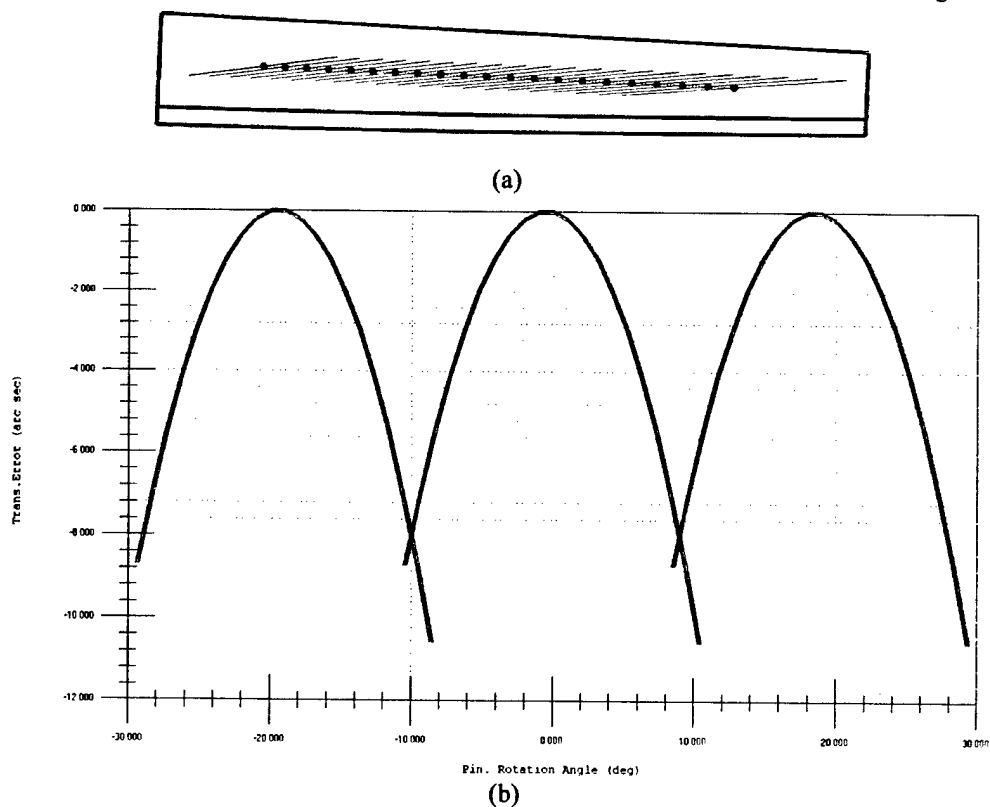
Figure 2.5. (a) Path of contact and (b) function of transmission errors for FTD2 design.

2.4 Investigation of Limits and Tolerances to Errors of Alignment

The limits and tolerances for absorption of errors of alignment have been investigated for the previously mentioned five cases of design. The limits of the values of errors of alignment that can be absorbed by the gear drive are those that make the path of contact for one cycle of meshing to have one contact point on the edge of the gear tooth surface (see Fig. 2.6). Tables 2.1 to 2.5 show the limits and tolerances to errors of alignment for the five cases of design represented above.

Table 2.1. Limits and tolerances to errors of alignment for the case of design GTD1.

Name of Parameters	Pinion concave-Gear convex		
	Min.	Max.	Tolerance
Axial Displacement of the pinion, ΔA_1 (mm)	-0.02 mm	0.45 mm	0.47 mm
Axial Displacement of the gear, ΔA_2 (mm)	-0.23 mm	0.55 mm	0.78 mm
Shortest distance between axes of pinion and gear, ΔE (mm)	0.08 mm	0.30 mm	0.22 mm
Change of crossing angle, $\Delta \gamma$ (deg)	-0.09 deg	0.40 deg	0.49 deg

Table 2.2. Limits and tolerances to errors of alignment for the case of design GTD2.

Name of Parameters	Pinion concave-Gear convex		
	Min.	Max.	Tolerance
Axial Displacement of the pinion, ΔA_1 (mm)	-0.15 mm	0.40 mm	0.55 mm
Axial Displacement of the gear, ΔA_2 (mm)	-0.15 mm	0.90 mm	1.05 mm
Shortest distance between axes of pinion and gear, ΔE (mm)	0.11 mm	0.35 mm	0.24 mm
Change of crossing angle, $\Delta \gamma$ (deg)	-0.13 deg	0.36 deg	0.49 deg

Table 2.3. Limits and tolerances to errors of alignment for the case of design GTD3.

Name of Parameters	Pinion concave-Gear convex		
	Min.	Max.	Tolerance
Axial Displacement of the pinion, ΔA_1 (mm)	-0.16 mm	0.37 mm	0.53 mm
Axial Displacement of the gear, ΔA_2 (mm)	-0.11 mm	0.68 mm	0.79 mm
Shortest distance between axes of pinion and gear, ΔE (mm)	0.10 mm	0.35 mm	0.25 mm
Change of crossing angle, $\Delta \gamma$ (deg)	-0.16 deg	0.33 deg	0.49 deg

Table 2.4. Limits and tolerances to errors of alignment for the case of design FTD1.

Name of Parameters	Pinion concave-Gear convex		
	Min.	Max.	Tolerance
Axial Displacement of the pinion, ΔA_1 (mm)	-0.05 mm	0.06 mm	0.11 mm
Axial Displacement of the gear, ΔA_2 (mm)	-0.05 mm	0.10 mm	0.15 mm
Shortest distance between axes of pinion and gear, ΔE (mm)	-0.03 mm	0.03 mm	0.06 mm
Change of crossing angle, $\Delta \gamma$ (deg)	-0.09 deg	0.07 deg	0.16 deg

Table 2.5. Limits and tolerances to errors of alignment for the case of design FTD2.

Name of Parameters	Pinion concave-Gear convex		
	Min.	Max.	Tolerance
Axial Displacement of the pinion, ΔA_1 (mm)	-0.10 mm	0.10 mm	0.20 mm
Axial Displacement of the gear, ΔA_2 (mm)	-0.08 mm	0.10 mm	0.18 mm
Shortest distance between axes of pinion and gear, ΔE (mm)	-0.04 mm	0.05 mm	0.09 mm
Change of crossing angle, $\Delta \gamma$ (deg)	-0.12 deg	0.11 deg	0.23 deg

(a)

(b)
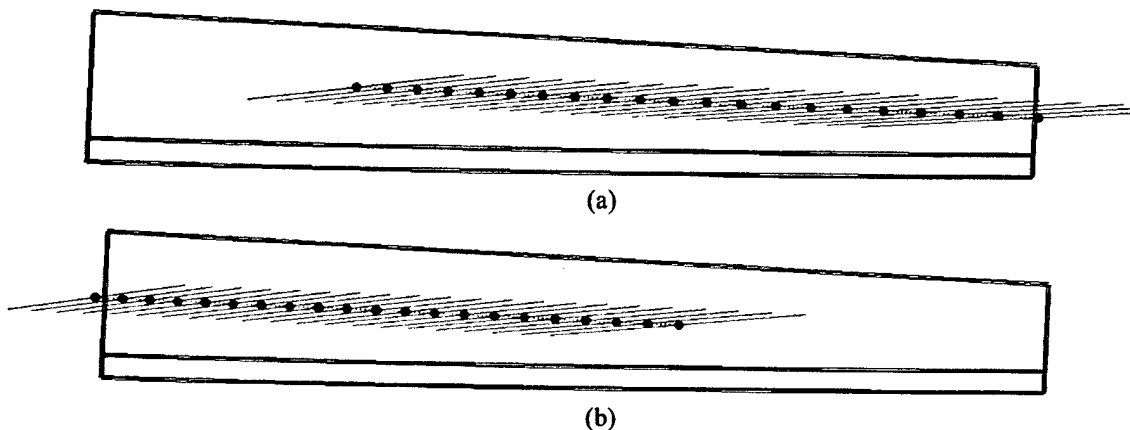
Figure 2.6. Case of design FTD2: shift of the bearing contact for (a) shortest distance between axes of pinion and gear ΔE = -0.04 mm and (b) shortest distance between axes of pinion and gear ΔE = 0.05 mm.

For cases of design GTD1, GTD2, and GTD3, the following errors of alignment have been compensated in generation:

Axial displacement of the pinion, ΔA_1 = 0.23 mm.

Shortest distance between axes of pinion and gear, ΔE = 0.16 mm.
Change of crossing angle, $\Delta \gamma$ = 0.121 deg.

No errors of alignment have been compensated for cases of design FTD1 and FTD2. However, this capability is available in the developed computer program.

Figure 2.7 shows a graph with the tolerances to errors of alignment for the five cases of design considered. The following conclusions can be drawn from the obtained tolerances to errors of alignment:

(i)   Formate-cut spiral bevel gear drives (designs FTD1 and FTD2) are more sensitive to all the different types of alignment errors than generated spiral bevel gear drives (designs GTD1, GTD2, and GTD3).

(ii) Spiral bevel gear drives are very sensitive to error of alignment ΔE .

(iii) The more mismatch between the profiles of the head-cutters, the less sensitivity to errors of alignment (see tolerances for cases FTD1 and FTD2).
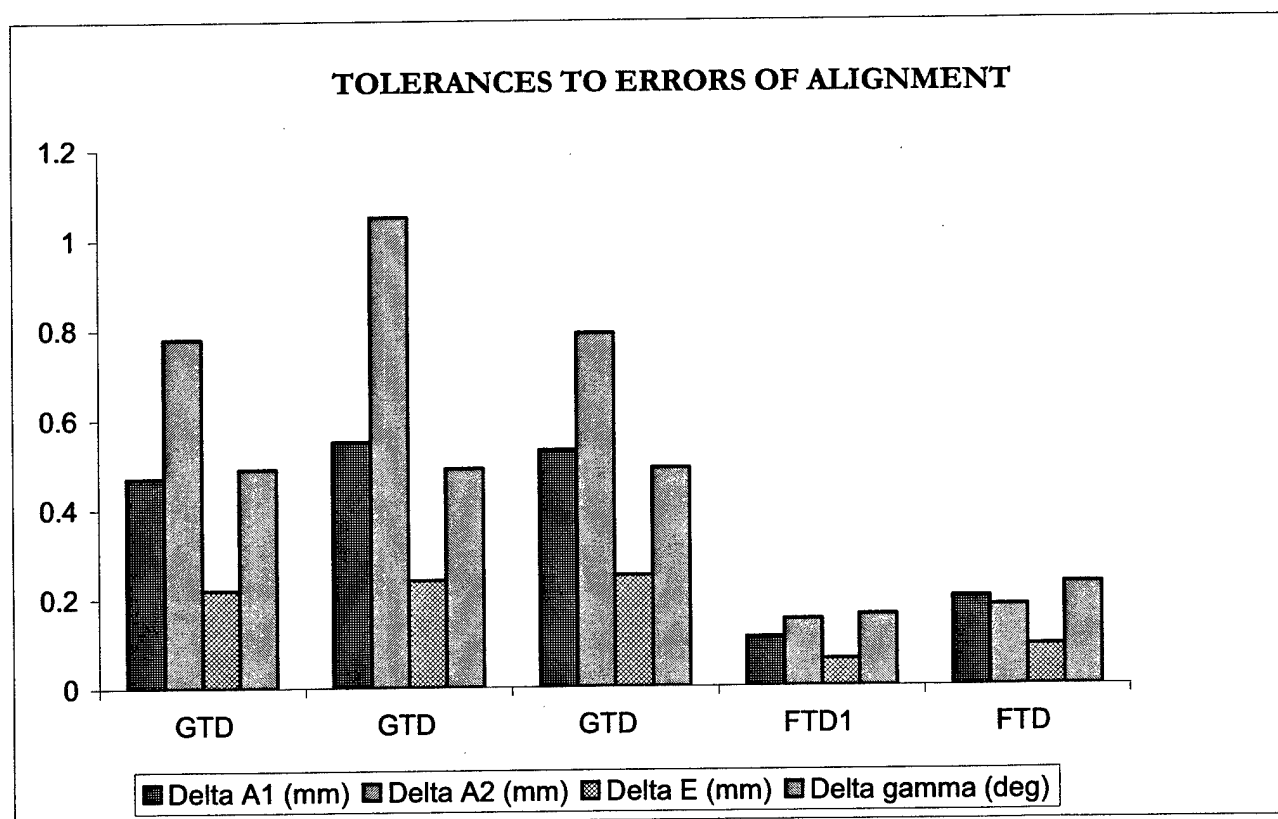
Figure 2.7. Tolerances to errors of alignment for five cases of design for generated and formate cut spiral bevel gear drives.

As shown in Figure 2.7, spiral bevel gear drives are very sensitive to the change of the shortest distance between axes, ΔE . A method to compensate the shift of the path of contact caused by error of alignment ΔE is proposed. This method is based on compensation of error of alignment ΔE by the axial displacement of the pinion ΔA_1 . Figure 2.8 shows an example of compensation of error of alignment error of alignment ΔE for the case of a formate cut spiral bevel gear drive. The case of design FTD2 has been considered for the compensation shown in Figure 2.8.

Figure 2.8(a) shows the path of contact when no errors of alignment occur. Figure 2.8(b) shows the path of contact for an error of alignment ΔE =0.04 mm. Figure 2.8(c) shows the path of contact for an error of alignment ΔE =0.04 mm along with an axial displacement of the pinion ΔA_1 =0.15 mm. As shown in Figure 2.8(c), an axial displacement of the pinion can compensate the shift of the path of contact caused by the shortest distance between axes ΔE . The same compensation can be achieved with face-milled generated spiral bevel gears.

Figure 2.8(d) shows the function of transmission errors when error of alignment ΔE =0.04 mm is compensated with an axial displacement of the pinion ΔA_1 =0.15 mm. The transmission errors are of parabolic shape with a maximum level of 8.8 arcsec.
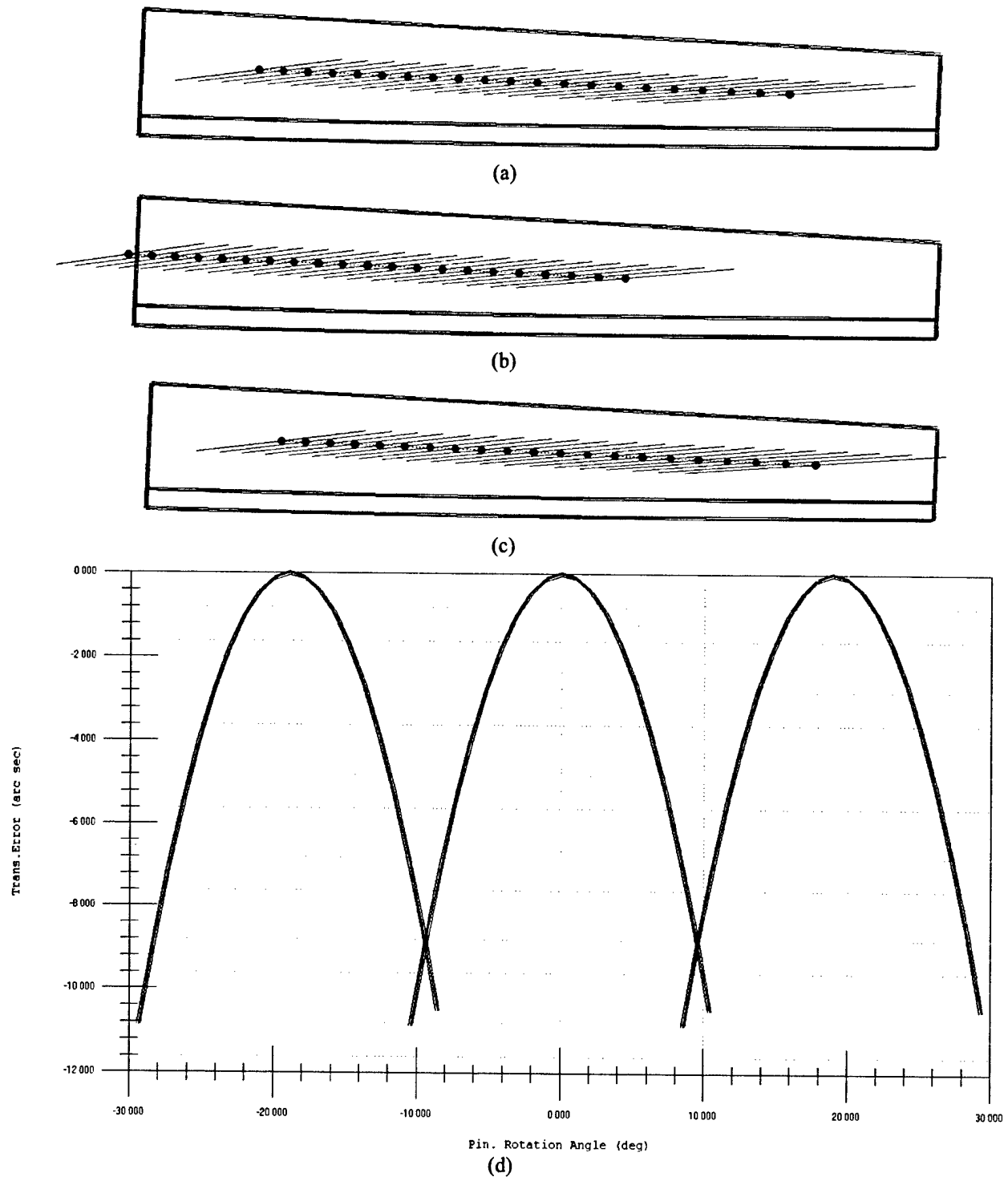

(a)

(b)

(c)

(d)

Figure 2.8. Case of design FTD2: (a) path of contact when no errors of alignment occur, (b) path of contact for error of alignment ΔE =0.04 mm, (c) path of contact when error of alignment ΔE =0.04 mm is compensated by ΔA_1 =0.15 mm, (d) function of transmission errors for conditions of item (c).

2.5 Enhanced Approach for Finite Element Analysis (FEA)

Application of finite element analysis permits:

- Determination of contact and bending stresses for pinion and gear.

- Investigation of formation of bearing contact and transfer of load to the next contacting pair of teeth.

- Investigation of existence of hidden areas of edge contact in high-loaded gear drives.

Finite element analysis has been performed by application of the general purpose computer program ABAQUS.

An enhanced approach for performing of finite element analysis that has the following advantages has been developed:

(a) The same programming language (FORTRAN) is applied for synthesis, analysis, and generation of finite element models of the gear drives. Graphical interpretation of the output is obtained by using the Visual Fortran Quick Win run time library.

(b) The generation of the finite element mesh required for finite element analysis is performed automatically using the equations of the surfaces of the tooth and the portion of the rim. Nodes of the finite element mesh lying on the tooth surfaces of pinion (gear) are guaranteed to be points of the real tooth surfaces of the pinion (gear). Loss of accuracy due to the development of solid models using CAD computer programs is avoided. The boundary conditions for the pinion and the gear are set automatically as well.

(c) Investigation of the bearing contact formation for the whole cycle of meshing permits the discovery of hidden areas of edge contact.

(d) There is no need to apply CAD computer programs for the development of finite element models required for application of general purpose FEA computer program ABAQUS.

The development of the solid models and finite element meshes using CAD computer programs is time expensive, requires skilled users of used computer programs and has to be done for every case of gear geometry and position of meshing desired to be investigated.

The developed approach is free of all these disadvantages and is summarized as follows:

Step 1: Using the equations of both sides of tooth surfaces and the portions of the corresponding rim, we may represent analytically the volume of the designed body. Figure 2.9(a) shows the designed body for one-tooth model of the pinion of a spiral bevel gear drive.

Step 2: Auxiliary intermediate surfaces 1 to 6 as shown in Fig. 2.9(b) can be determined. Surfaces 1 to 6 enable us to divide the tooth in six parts and control the discretization of these tooth subvolumes into finite elements.

Step 3: Analytical determination of node coordinates is performed taking into account the number of desired elements in longitudinal and profile direction (Fig. 2.9(c)). We emphasize that all nodes of the finite element mesh are determined analytically and those lying on the intermediate surfaces of the tooth are indeed points belonging to the real surface.

Step 4: Discretization of the model by finite elements using nodes determined in previous step is accomplished as shown in Fig. 2.9(d).
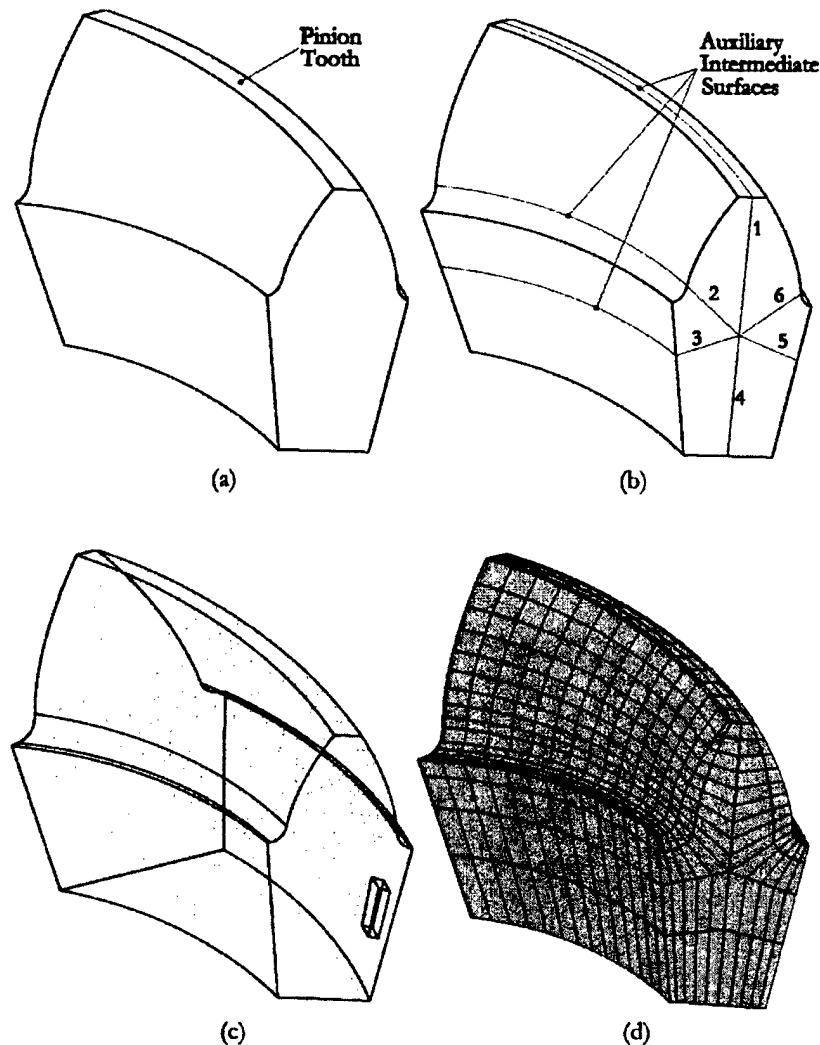
Figure 2.9. Illustrations of (a) the volume of designed body, (b) auxiliary intermediate surfaces, (c) determination of nodes for the whole volume, and (d) discretization of the volume by finite elements.

Step 5: Setting of boundary conditions for gear and pinion is performed automatically. Nodes on the sides and bottom part of the rim portion of the gear are considered fixed (Fig. 2.10(a)). Nodes on the two sides and bottom part of the rim portion of the pinion build a rigid surface (Fig. 2.10(b)). Rigid surfaces are three-dimensional geometric structures that cannot be deformed but can perform translation or rotation as rigid bodies. They are also very cost-effective since the variables associated with a rigid surface are the translations and rotations of a single node, known as the rigid body reference node (Fig. 2.10(b)). The rigid body reference node is located on the pinion axis of rotation with all degrees of freedom but the rotation around the axis of rotation of the pinion fixed to zero. The torque is applied directly to the remaining degree of freedom of the rigid body reference node (Fig. 2.10(b)).

Step 6: Definition of contacting surfaces for the contact algorithm of the finite element computer program ABAQUS is obtained automatically as well and requires definition of the master and slave surfaces. Generally, the master surface is chosen as the surface of the stiffer body or as the surface with the coarser mesh if the two surfaces are on structures with comparable stiffness. Finite element mesh for the pinion is more refined than the one for the gear due to larger curvatures. The gear and pinion tooth surfaces are considered as the master and slave surfaces respectively for the contact algorithm.
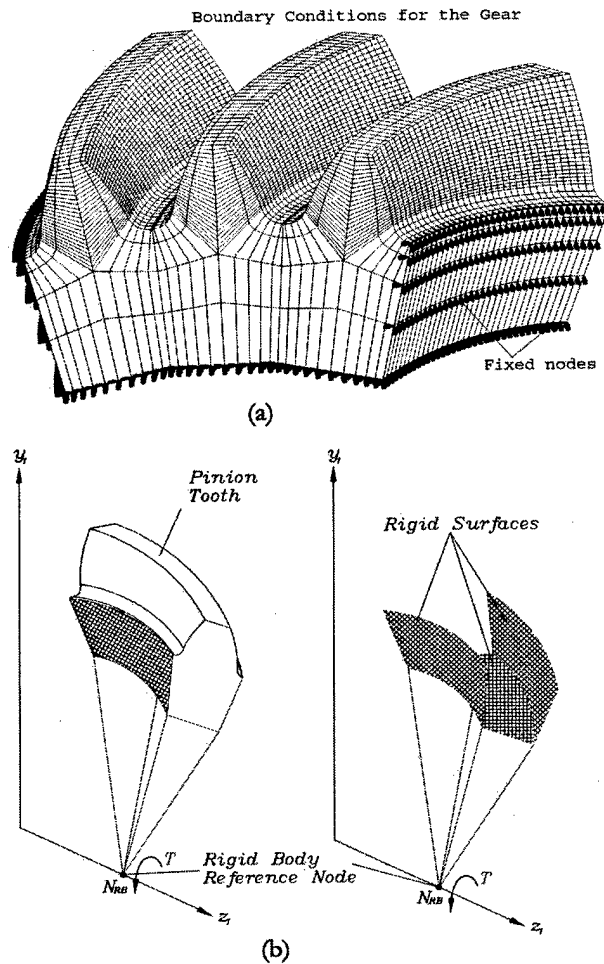
Figure 2.10. (a) Boundary conditions for the gear and (b) schematic representation of boundary conditions and application of torque for the pinion.

2.6 Results of FEA

Five cases of design of face-milled generated spiral bevel gear drives and formate cut spiral bevel gear drives have been accomplished.

The discretization of pinion and gear teeth for a 3-pair-of-teeth finite element model is shown in Fig. 2.11. Incompatible mode elements C3D8I have been used to build the finite element mesh. These elements are first-order elements that are enhanced by incompatible modes of deformation to improve their bending behavior. The total number of elements is 33606 with 42076 nodes for each geometric model. The material is steel with the properties of Young's Modulus $E=2.068 \cdot 10^8$ mN/mm^2 and the Poisson's ratio 0.29. A torque of 549 N·m has been applied to the pinion of the gear drives. The finite element mesh of the whole gear drive for case of design FTD1 is shown in Fig. 2.12.
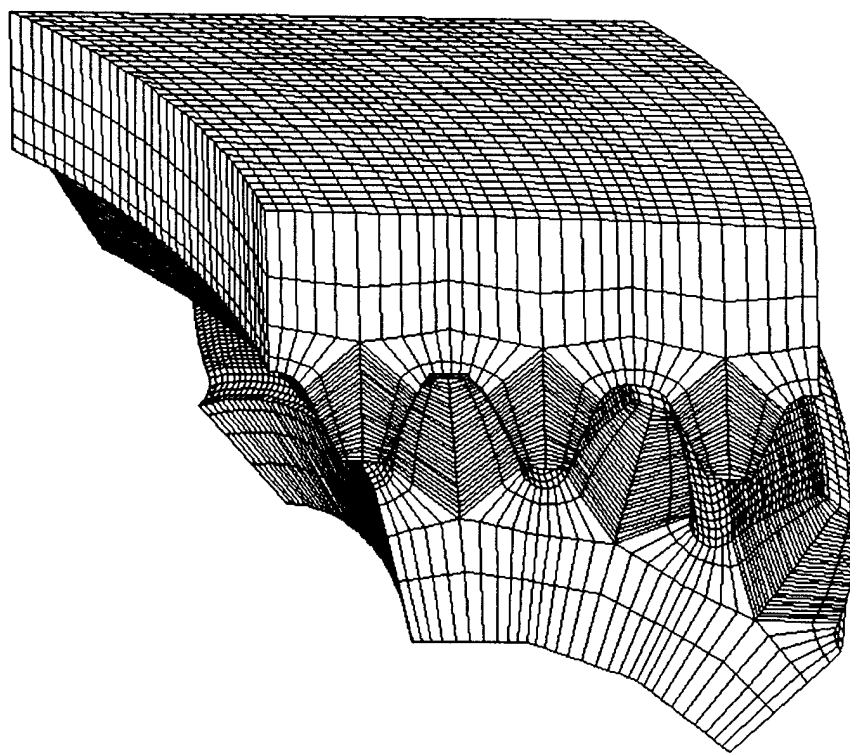
Figure 2.11. Finite element model of three pairs of contacting teeth used for FEA.
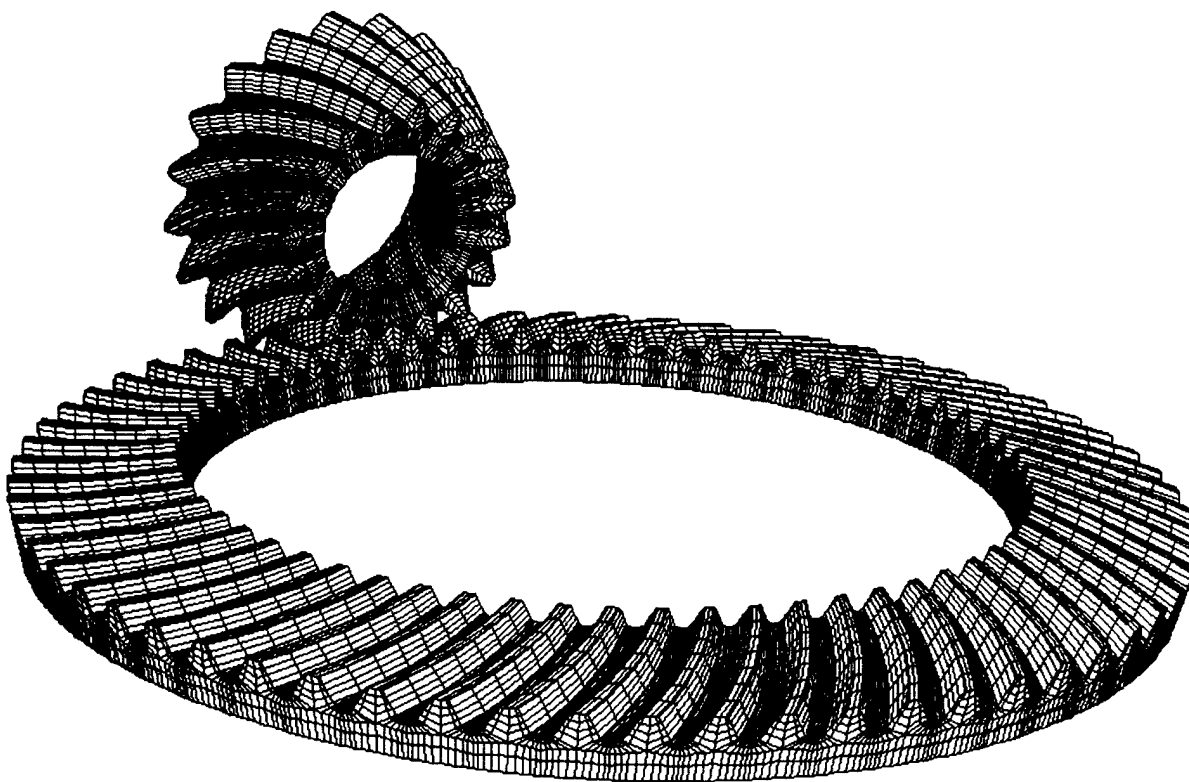
Figure 2.12. Whole finite element mesh of the formate-cut spiral bevel gear drive of design FTD1.

The concave side of the pinion and the convex side of the gear are considered as the driving and driven surfaces, respectively, for all cases of design.

The units used for stress distribution in Figures 2.13, 2.14, 2.17, and 2.18 are mN/mm^2. Von Mises stresses are represented wherein stresses are shown.

Figure 2.13 shows the contact stresses for the pinion of the generated spiral bevel gear drive of baseline design (GTD1) at contact point 17. Edge contact has been found. Design GTD2 wherein head-cutters of parabolic profiles have been used for gear generation and design GTD3 wherein head-cutters of parabolic profiles have been used for pinion generation permits the avoidance of edge contact all over the path of contact. Figure 2.14 shows the contact stresses for the pinion of the generated spiral bevel gear drive of case of design GTD3 at contact point 17 as well. Edge contact has been avoided indeed and contact stresses decreased from 1518 to 1175 MPa.

Figure 2.15 shows the evolution of contact stresses (Fig 2.15(a)) and bending stresses (Fig. 2.15(b)) for the pinion of cases of design GTD1, GTD2, GTD3. Edge contact has been avoided and contact stresses decreased for cases of design GTD2 and GTD3. However, case of design GTD3 permits the larger reduction of contact stresses during the cycle of meshing

Bending stresses are almost the same for the pinion of cases of design GTD1, GTD2, and GTD3. Only a very small reduction of bending stresses has been found for case of design GTD3. The larger bending stresses occurs at the mean contact point

Figure 2.16 shows the evolution of contact and bending stresses for the gear of cases of design GTD1, GTD2, and GTD3. Reduction of contact stresses could be obtained as well for cases of design GTD2 and GTD3 with respect to the baseline design GTD1 (see Fig. 2.16(a)). The bending stresses for the gear of all cases of design are almost the same. Larger bending stress occurs at the mean contact point as well.

Figures 2.17 and 2.18 show the contact stresses for the pinion and the gear, respectively, of case of design FTD1 wherein the gear is manufactured using the formate-cut method. Edge contact has been avoided for the whole path of contact for one cycle of meshing.

Figure 2.19 shows the evolution of contact and bending stresses for the pinion of cases of design FTD1, FTD2, and the baseline design GTD1. Contact and bending stresses for cases of design FTD1 and FTD2 have been reduced with respect to the baseline design GTD1. Also contact and bending stresses are lower for case of design FTD1 with respect to the case of design FTD2 wherein a smaller contact ellipse has been considered to increase the tolerances to errors of alignment.

Figure 2.20 shows the evolution of contact and bending stresses for the gear of cases of design FTD1, FTD2, and GTD1. Contact stresses obtained for the gear of case of design FTD1 are similar to those obtained for the baseline design GTD1. Case of design FTD2 yields larger contact stresses (see Fig. 2.20(a)). Bending stresses are lower for the gear of case of design FTD1.

Based on the obtained FEA results, the following conclusions can be obtained:

Application of head-cutters of parabolic profiles for generation of the gear or the pinion of face-milled generated spiral bevel gear drives permits the avoidance of hidden areas of edge contact for high-loaded gear drives.

The application of head-cutters of parabolic profiles for generation of the pinion is more effective than its application for generation of the gear for avoidance of edge contact and reduction of contact stresses (see Figure 2.15(a)).

Using the formate-cut method and a head-cutter of parabolic profile, a suitable design could be found for the spiral bevel gear 19 x 62 with longitudinal path of contact, no edge contacts, and low level of contact and bending stresses.

Designs FTD1 and FTD2 based on the formate-cut method for grinding of the gear, yield lower level of contact and bending stresses with respect to the baseline design based on the generated method for the gear (see Figures 2.19 and 2.20).

Design FTD1 wherein a larger contact ellipse than the one corresponding to design FTD2 was designed yields the lower contact and bending stresses (see Figures 2.19 and 2.20).
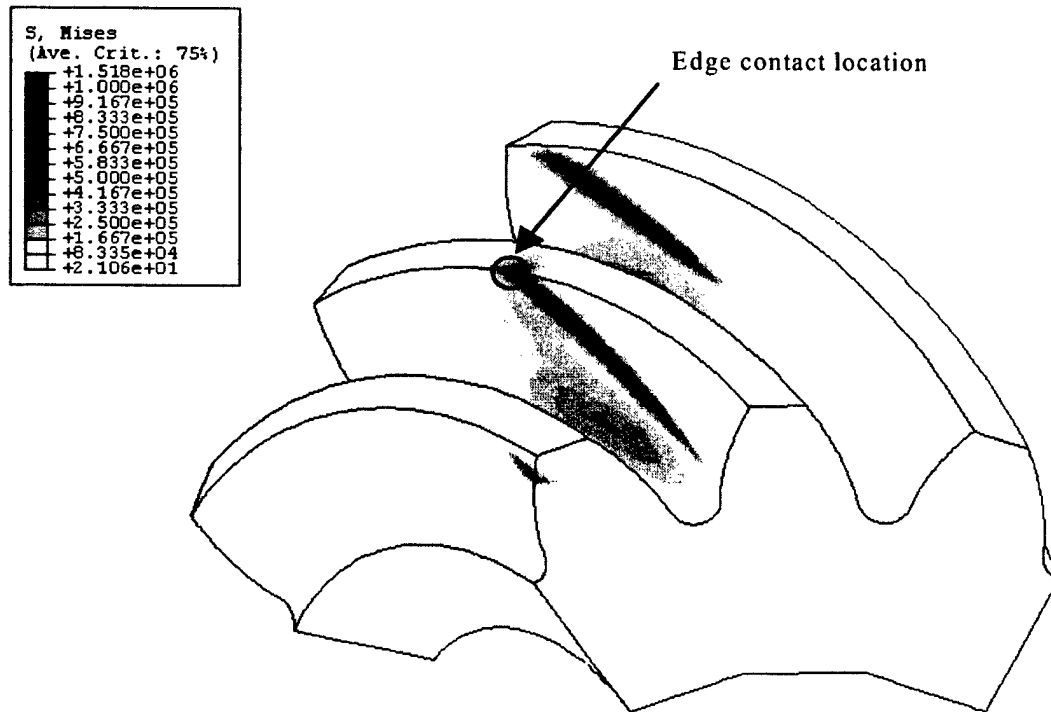

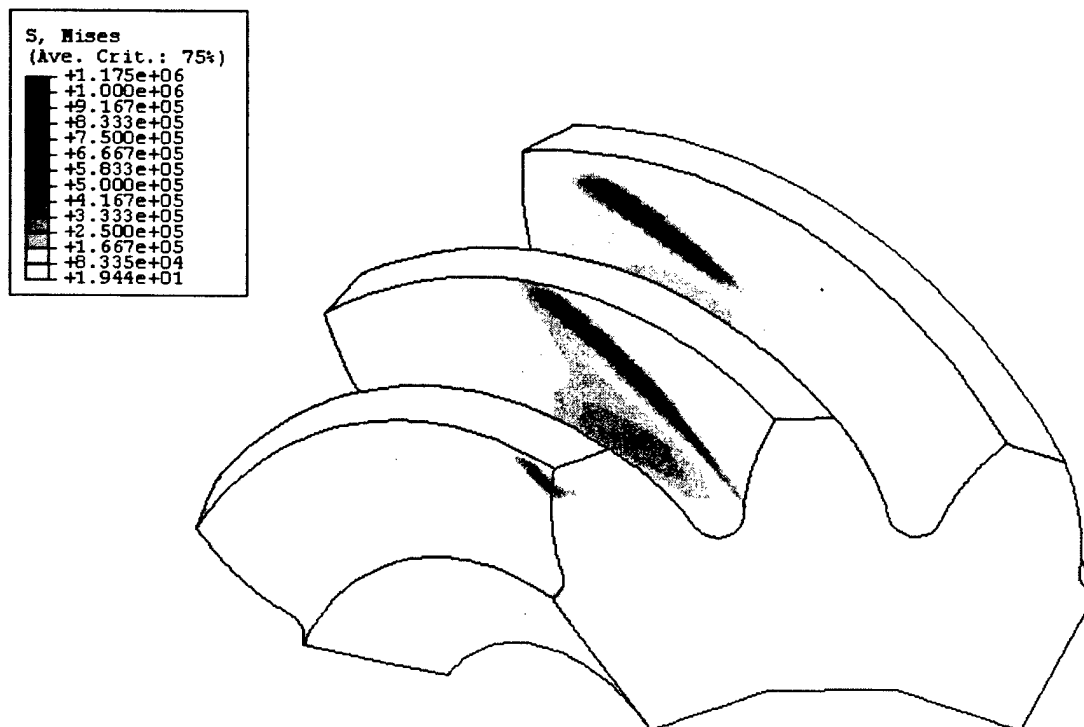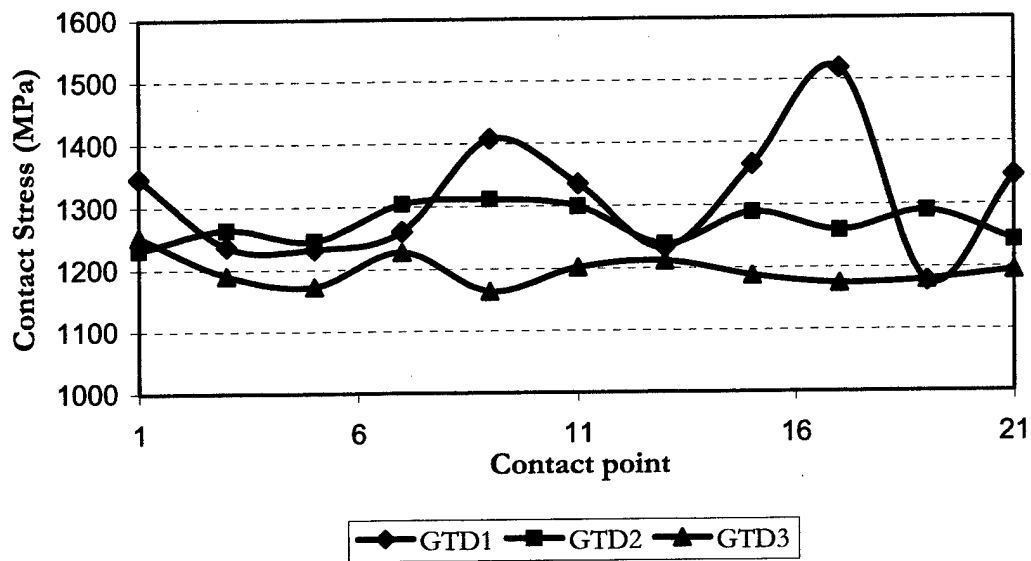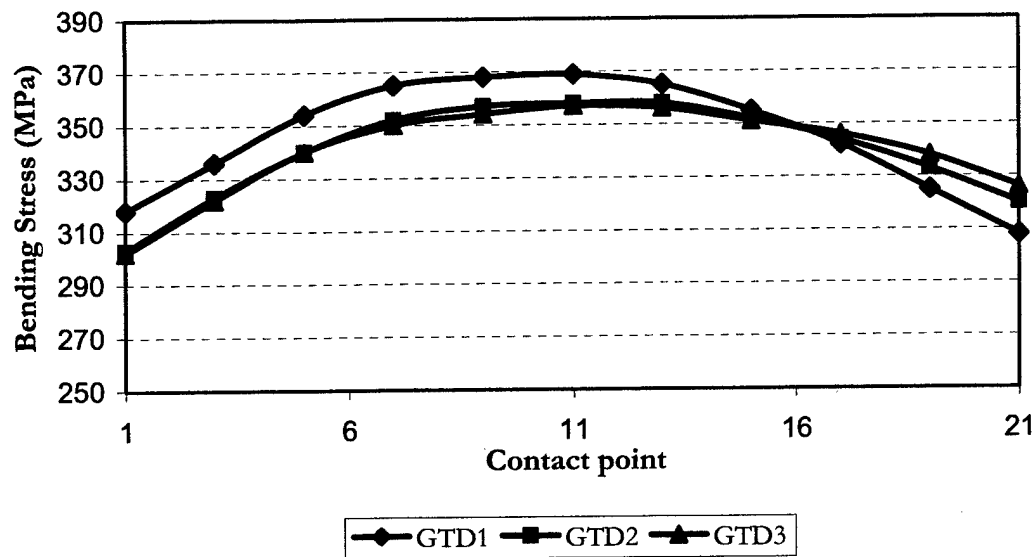Figure 2.13. Contact stresses for the pinion at contact point 17 for baseline design (GTD1).

Figure 2.14. Contact stresses for the pinion at contact point 17 for case of design GTD wherein the pinion is generated with head-cutters of parabolic profiles.
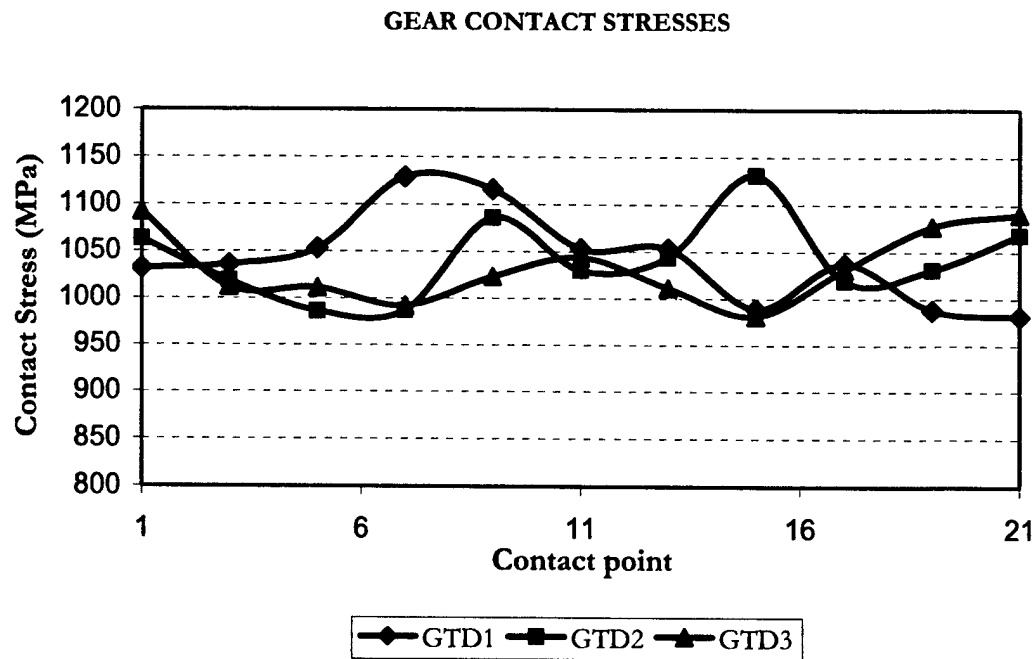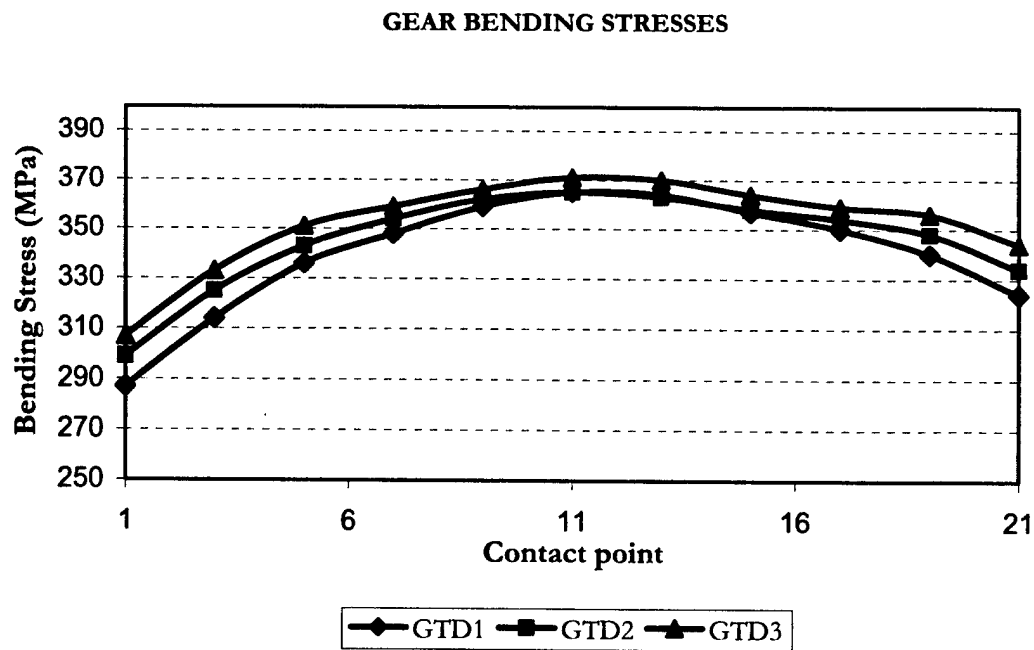
PINION CONTACT STRESSES

(a)

PINION BENDING STRESSES

(b)

Figure 2.15. Evolution of (a) contact stresses and (b) bending stresses for the pinion of cases of design GTD1, GTD2, GTD3.

GEAR CONTACT STRESSES

(a)

GEAR BENDING STRESSES

(b)

Figure 2.16. Evolution of (a) contact stresses and (b) bending stresses for the gear of cases of design GTD1, GTD2, and GTD3.
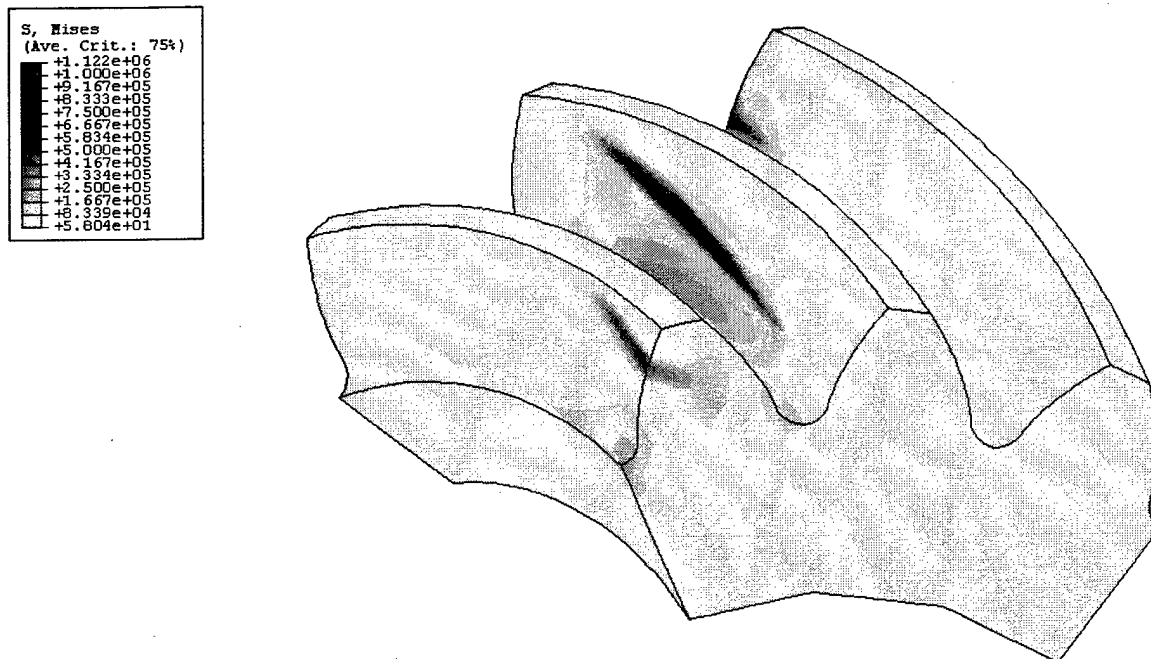
Figure 2.17. Contact stresses for the pinion at the mean contact point for case of design FTD1
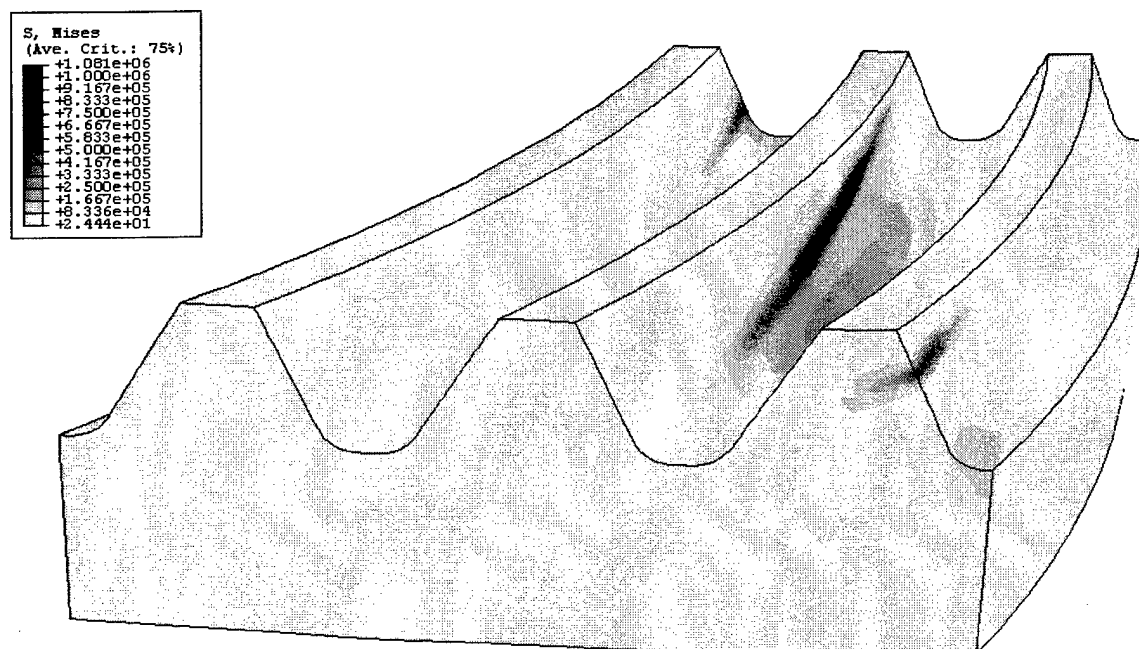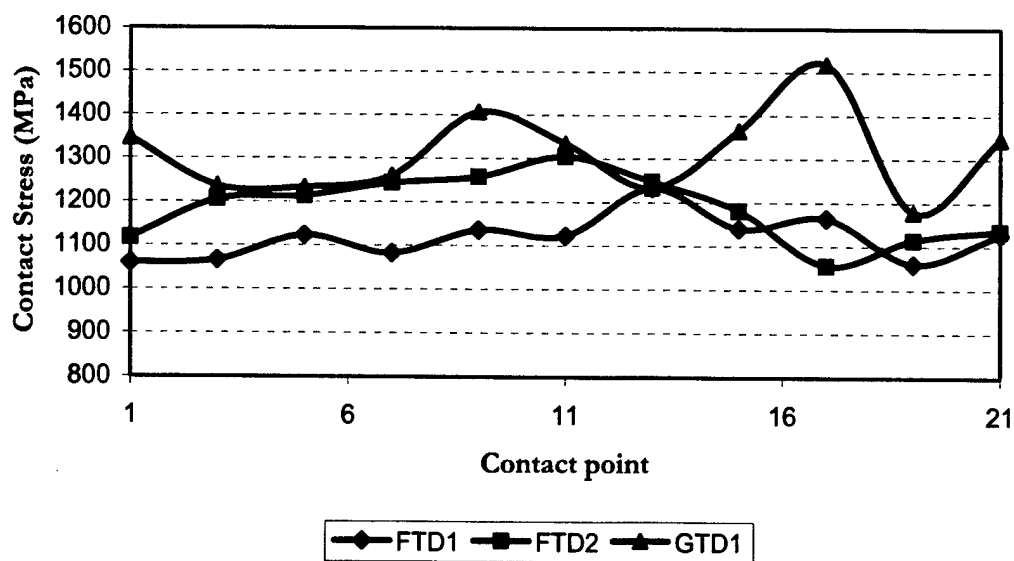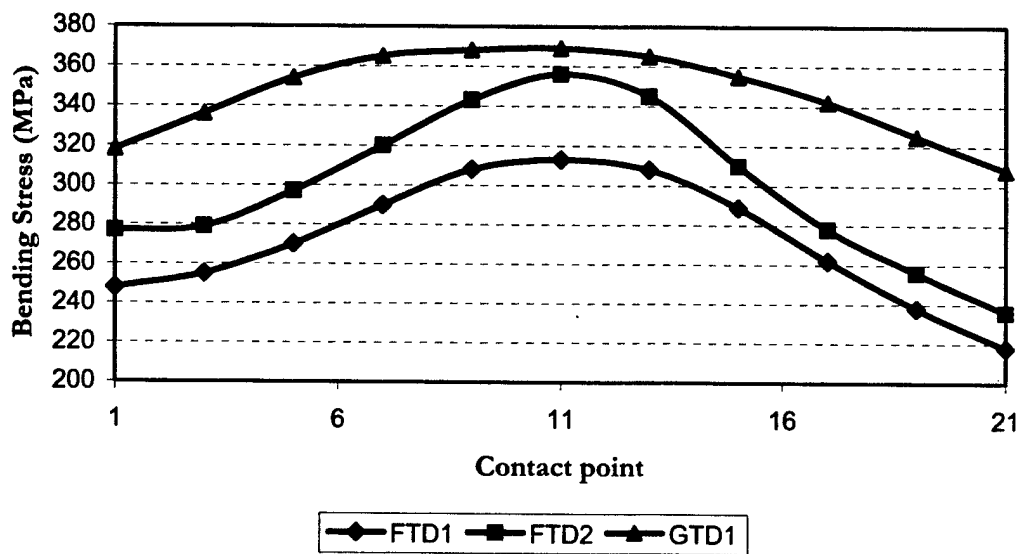wherein the gear is manufactured by the formate-cut method.

Figure 2.18. Contact stresses for the formate-cut gear at the mean contact point for case of design FTD1.
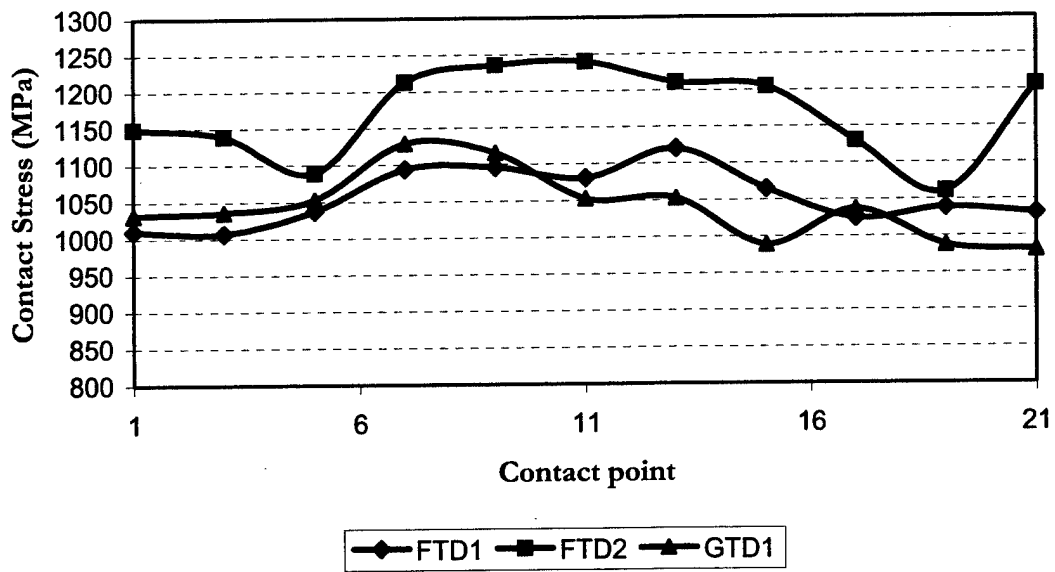
PINION CONTACT STRESSES
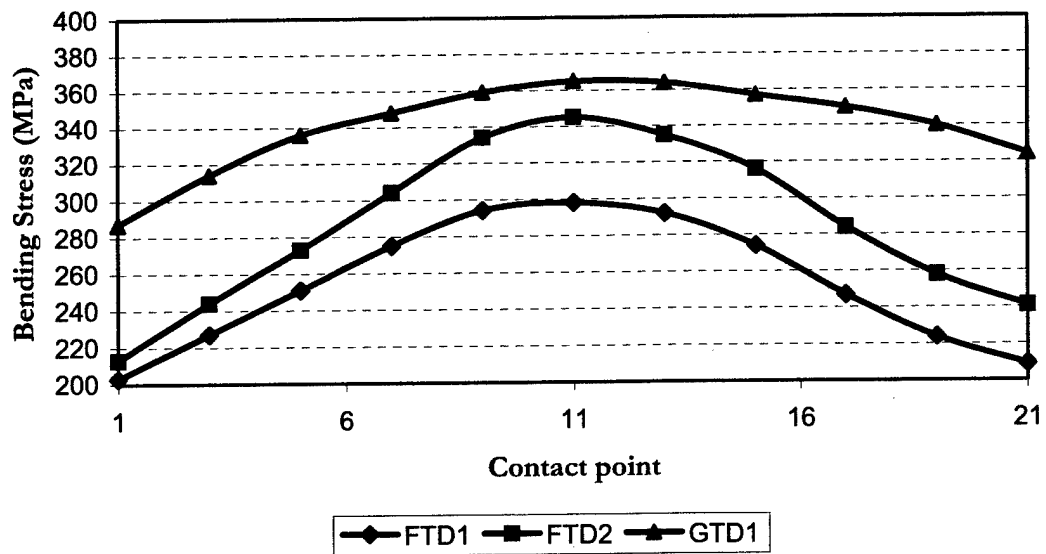

(a)

PINION BENDING STRESSES

(b)

Figure 2.19. Evolution of (a) contact stresses and (b) bending stresses for the pinion of cases of design FTD1, FTD2, and baseline design GTD1.

GEAR CONTACT STRESSES

(a)

GEAR BENDING STRESSES

(b)

Figure 2.20. Evolution of (a) contact stresses and (b) bending stresses for the gear
of cases of design FTD1, FTD2, and baseline design GTD1.

Chapter 3

Conclusions

Based on the research performed, the following conclusions can be obtained:

- A new computer program has been developed that enables to provide optimized machine-tool settings for finishing of spiral bevel gears utilizing the "Formate" grinding process. Such settings provide minimized transmission errors at a low level and a stable bearing contact adjusted for assigned misalignment. The computer program developed is based on the following basic ideas:
  - o Application of a parabolic function of transmission errors for reduction of noise and vibration.
  - o Optimization of machine-tool settings for the formate grinding method, including application of parabolic cutter blade profiles.
  - o Application of an enhanced approach for automatic development of finite element models and stress analysis

- The developed approach of design, generation, simulation of meshing and contact, and stress analysis of formate cut spiral bevel gear drives has been successfully applied for the design of a formate cut spiral bevel gear drive with a stabilized bearing contact and favorable shape of transmission errors of low magnitude.

- A formate cut spiral bevel gear drive has been designed considering as a reference a design based on face-milled generated spiral bevel gear drives. The provided design allows to increase the productivity of manufacturing of the gears by the formate cut method, avoid edge contacts, and reduce contact and bending stresses.

- Head-cutters with parabolic profiles have been applied for the generation of the gear of formate cut gear drives and for generation of pinion and gear of face-milled generated spiral bevel gear drives. Application of head-cutters with parabolic profiles allows us to increase the mismatch between generating surfaces of pinion and gear and avoid the appearance of edge contact.

- Automatic generation of finite element models have been developed to perform multi-tooth stress analysis for several contact points along the path of contact and obtain the evolution of contact and bending stresses. Hidden areas of edge-contact for high-loaded gear drives are detected if they exist.

- A method for compensation of the shift of the path of contact caused by a change of the shortest distance between the axis of the pinion and the gear, ΔE, has been proposed. It is based on the compensation of error of alignment ΔE by the axial displacement of the pinion, ΔA_1.

Preceding Page Blank

References

[1]   Litvin, F.L., 1960, 1968, Theory of Gearing, 1st ed. (1960), 2nd ed. (1968). Nauka (in Russian).

[2]   Litvin, F.L., 1969, "Die Beziehungen Zwischen den Krümmungen der Zahnoberflächen bei Räumlichen Verzahnungen". Z. Angew. Math. Mech. 49: 685-690 (in German).

[3]   Litvin, F.L. Rahman P. and Goldrich R.N., 1982, "Mathematical Models for the Synthesis and Optimization of Spiral Bevel Gear Tooth Surfaces", NASA CR-3553.

[4]   Litvin, F.L., 1989, Theory of Gearing, NASA Reference Publication 1212.

[5]   Litvin, F.L. and Zhang, Y., 1991, "Local Synthesis and Tooth Contact Analysis of Face-Milled Spiral Bevel Gears", NASA Contractor Report 4342, AVSCOM Technical Report 90-C-028.

[6]   Lewicki, D.G., Handschuh, R.F., Henry, Z.S. and Litvin, F.L., 1994, "Low-Noise, High-Strength, Spiral-Bevel Gears for Helicopter Transmissions", Journal of Propulsion and Power, Vol. 10, No. 3.

[7]   Litvin, F.L., 1994, Gear Geometry and Applied Theory, Prentice Hall.

[8]   Litvin, F.L. and Zhao, X., 1996, "Computerized Design and Analysis of Face-milled, Uniform Tooth Height, Low-Noise Spiral Bevel Gear Drives", NASA Contractor Report 4704.

[9]   Litvin, F.L., Wang, A.G., and Handschuh R.F., 1996, "Computerized Design and Analysis of Face-Milled, Uniform Tooth Height Spiral Bevel Gear Drives", Journal of Mechanical Design, Vol. 118, pp. 573-579.

[10] Zalgaller, V.A., 1975, Theory of Envelopes, Nauka, Moscow (in Russian).

[11] Zhang, Y., Litvin, F.L., and Handschuh R.F., 1995, "Computerized Design of Low-Noise Face-Milled Spiral Bevel Gears", Mech. Mach. Theory, Vol. 30, No. 8, pp. 1171-1178.

[12] F. L. Litvin, A. G. Wang and R. F. Handschuh, "Computerized Generation and Simulation of Meshing and Contact of Spiral Bevel Gears with Improved Geometry", J. Comput. Methods Appl. Mech. Engrg. and 158 (1998) 35-64.

[13] Press, William H., et al, Numerical Recipes in Fortran 77, The Art of Scientific Computing, Cambridge University Press, New York, 2nd Edition, 1992.

[14] IMSL Fortran 90 MP Library, v. 3.0, Visual Numerics, Inc., 1998.

[15] Argyris, J., Fuentes, A., Litvin, F. L., "Computerized Integrated Approach for Design and Stress Analysis of Spiral Bevel Gears", J. Comput. Methods Appl. Mech. Engrg., 191 (2002) 1057-1095.

[16] Litivn, F. L., Fuentes, A., Fan, Q., Handschuh, R. F., "Computerized Design, Simulation of Meshing and Contact and Stress Analysis of Face-Milled Formate Generated Spiral Bevel Gears", Mechanism and Machine Theory, 37 (2002) 441-459.

[17] Litvin, F. L., Fan. Q., Fuentes, A., 2001, "Computerized Design, Generation, and Simulation of Meshing and Contact of Face-Milled Formate Cut Spiral Bevel Gears", NASA/CR- 2001-210894, ARL-CR-467

REPORT DOCUMENTATION PAGE

Public reporting burden for this collection of information is estimated to average 1 hour per response, including the time for reviewing instructions, searching existing data sources, gathering and maintaining the data needed, and completing and reviewing the collection of information. Send comments regarding this burden estimate or any other aspect of this collection of information, including suggestions for reducing this burden, to Washington Headquarters Services, Directorate for Information Operations and Reports, 1215 Jefferson Davis Highway, Suite 1204, Arlington, VA 22202-4302, and to the Office of Management and Budget, Paperwork Reduction Project (0704-0188), Washington, DC 20503.

1. AGENCY USE ONLY (Leave blank)	2. REPORT DATE June 2003	3. REPORT TYPE AND DATES COVERED Final Contractor Report

4. TITLE AND SUBTITLE

Computerized Design, Generation, Simulation of Meshing and Contact, and Stress Analysis of Formate Cut Spiral Bevel Gear Drives

5. FUNDING NUMBERS

WBS-22-708-28-02
NAG3-2450
1L162211A47A

6. AUTHOR(S)

Faydor L. Litvin, Alfonso Fuentes, Baxter R. Mullins, and Ron Woods

7. PERFORMING ORGANIZATION NAME(S) AND ADDRESS(ES)

University of Illinois at Chicago
Department of Mechanical and Industrial Engineering
835 S. Wolcott Ave.
Chicago, Illinois 60607-7022

8. PERFORMING ORGANIZATION REPORT NUMBER

E-13931

9. SPONSORING/MONITORING AGENCY NAME(S) AND ADDRESS(ES)

National Aeronautics and Space Administration
Washington, DC 20546-0001
and
U.S. Army Research Laboratory
Adelphi, Maryland 20783-1145

10. SPONSORING/MONITORING AGENCY REPORT NUMBER

NASA CR—2003-212336
ARL-CR-525

11. SUPPLEMENTARY NOTES

12a. DISTRIBUTION/AVAILABILITY STATEMENT

Unclassified - Unlimited
Subject Category: 37   Distribution: Nonstandard

Available electronically at http://gltrs.grc.nasa.gov

This publication is available from the NASA Center for AeroSpace Information, 301-621-0390.

12b. DISTRIBUTION CODE

13. ABSTRACT (Maximum 200 words)

A new approach for design, generation, computerized simulation of meshing and contact, and stress analysis of formate cut spiral bevel gear drives is reported. The approach proposed is based on application of four procedures that permit in sequence to provide a longitudinally directed bearing contact, a predesigned parabolic function of transmission errors, a limit to the shift of bearing contact caused by errors of alignment, and to automatically generate the finite element models for application of a general purpose finite element analysis computer program. A new computer program has been developed that provides optimized machine-tool settings for finishing of spiral bevel gears utilizing the "Formate" grinding process with minimized transmission errors. The new computer program is based on the four procedures mentioned above. The developed theory is illustrated with several examples of design and computations.

14. SUBJECT TERMS

Gears; Transmissions

15. NUMBER OF PAGES

61

16. PRICE CODE

17. SECURITY CLASSIFICATION OF REPORT	18. SECURITY CLASSIFICATION OF THIS PAGE	19. SECURITY CLASSIFICATION OF ABSTRACT	20. LIMITATION OF ABSTRACT
Unclassified	Unclassified	Unclassified	

NSN 7540-01-280-5500

Standard Form 298 (Rev. 2-89)
Prescribed by ANSI Std. Z39-18
298-102